Hydrodynamics in a gravel beach and its impact on the *Exxon Valdez* oil

Qiaona Guo,[1,2,3] Hailong Li,[1] Michel C. Boufadel,[2] and Youness Sharifi[2]

Received 24 February 2010; revised 28 July 2010; accepted 28 September 2010; published 31 December 2010.

[1] This paper investigated the interaction of groundwater and seawater in a tidally influenced gravel beach. Field observations of water table, pore water salinity were performed. The two-dimensional finite element model MARUN was used to simulate observed water table and salinity. Based on field observations and model calibrations, a two-layered beach structure was identified which is characterized by a high-permeability surface layer underlain by a low-permeability lower layer. The salt wedge seaward of the low tide line was almost invariant in comparison with the strong fluctuations of the salinity plume in the surface layer of the intertidal zone. The presence of the two layers prevented the presence of a freshwater discharge "tube" between the upper saline plume and salt wedge. This is in contrast with the previous works where freshwater discharge tube was observed. The tide-induced submarine groundwater discharge (SGD) was estimated at 9 m^3 d^{-1} m^{-1}, a large value that is probably due to the large tidal range of ~4.8 m and the very permeable surface layer. The freshwater-seawater dynamics revealed here may provide new insights into the complexity, intensity, and time scales of mixing between fresh groundwater and seawater in tidal beaches. The simulated water table of the beach was higher than the interface between the surface layer and the lower layer, which prevented *Exxon Valdez* oil from penetrating into the lower layer in 1989.

Citation: Guo, Q., H. Li, M. C. Boufadel, and Y. Sharifi (2010), Hydrodynamics in a gravel beach and its impact on the *Exxon Valdez* oil, *J. Geophys. Res.*, *115*, C12077, doi:10.1029/2010JC006169.

1. Introduction

[2] Beach zones are dynamic areas with complex interactions among physical, chemical, and biological components in the presence of exchange of saltwater and freshwater. Understanding beach hydrodynamics is a crucial step for a variety of investigations, such as understanding the ecology and biodiversity of nearshore groundwater systems [e.g., *McLachlan and Turner*, 1994; *Miller and Ullman*, 2004; *Li et al.*, 2005], determining beach accretion and erosion [*Horn*, 2002], quantifying chemical transfer from aquifer to water bodies [e.g., *Li et al.*, 1999; *Moore*, 1999], and controlling saltwater intrusion and mitigating the effects of nutrients and other chemicals on coastal environments [e.g., *Ataie-Ashtiani et al.*, 1999; *Boufadel et al.*, 1999a; *Boufadel*, 2000]. In particular, such a knowledge is needed for analyzing mechanisms causing persistence of subsurface oil spills [*Short et al.*, 2004, 2006] and for implementing bioremediation on the oil spills [*Venosa et al.*, 1996; *Boufadel et al.*, 2006, 2007; *Brovelli et al.*, 2007; *Li et al.*, 2007; *Eljamal et al.*, 2008].

[3] Beach groundwater flow has been intensively addressed in the literature. *Nielsen* [1990] derived an analytical solution for tidal dynamics of the water table in sandy beaches that took into account the effect of the sloping beach surface. *Turner* [1993] developed a numerical model SEEP to simulate the water table outcropping on macrotidal beaches. *Turner et al.* [1997] used the saturated flow numerical model MODFLOW to simulate the superelevation of groundwater in a tidally influenced laboratory beach. *Boufadel et al.* [1998] reported water table variation with tide in a laboratory beach. They modeled the measurements using the MARUN code [*Boufadel et al.*, 1999a]. *Robinson and Gallagher* [1999] used their saturated flow model to simulate water table in a tidally influenced beach. *Li et al.* [2000] derived an analytical solution for water table fluctuation in a coastal aquifer driven by spring-neap tides on a moving boundary that varies with the beach slope. *Ataie-Ashtiani et al.* [2001] used a numerical solution with sinusoidal tidal motion on a homogenous, mildly sloping beach to show tidal level impacts on beach hydrodynamics. *Teo et al.* [2003] developed a new analytical solution of higher order for water table fluctuations in coastal aquifers with sloping beaches. *Jeng et al.* [2005] derived an analytical solution for the spring-neap tide induced water table fluctuations in a sloping sandy beach, and compared their solution with field observations. *Cartwright et al.* [2006]

[1]School of Environmental Studies and (MOE) Biogeology and Environmental Geology Laboratory, China University of Geosciences, Wuhan, China.
[2]Department of Civil and Environmental Engineering, Temple University, Philadelphia, Pennsylvania, USA.
[3]School of Earth Sciences and Engineering, Hohai University, Nanjing, China.

0148-0227/10/2010JC006169

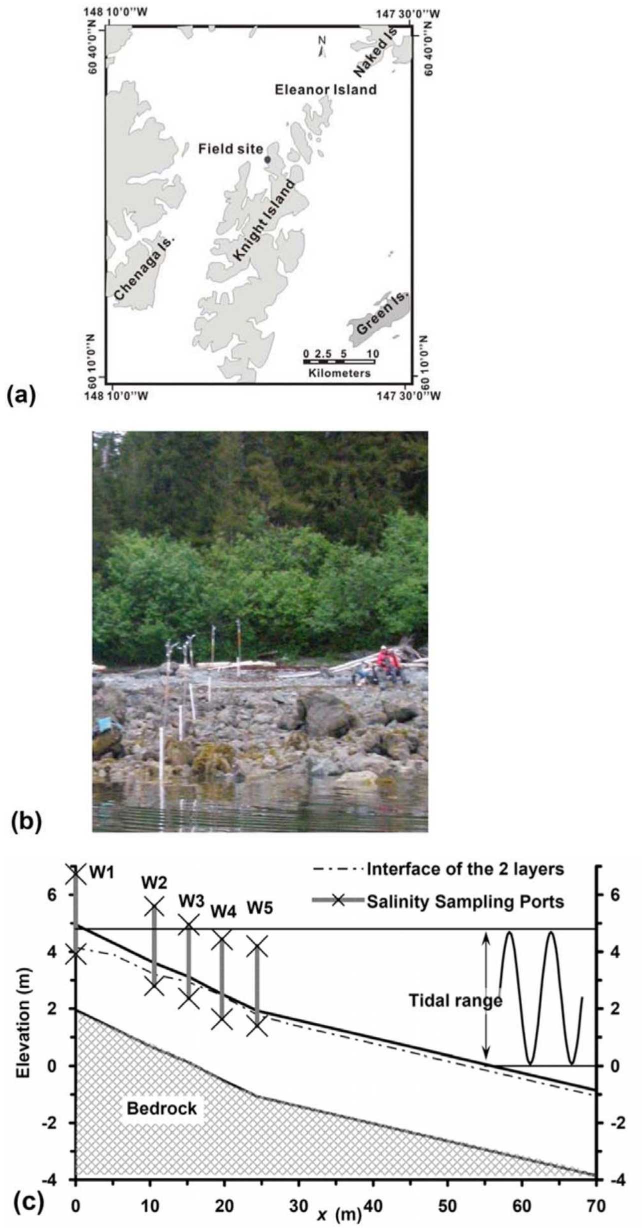

Figure 1. (a) Location of the studied beach on Knight Island, Alaska Prince William Sound. (b) Photograph of the beach KN-114A taken at low tide, the multiport salinity sampling wells (higher) and water table monitoring wells (lower) installed in the transect. Note the typical seaward increasing grain size distribution (pebbles at the high tide berms, cobbles on the upper platform, and boulders on the lower platform). (c) Cross-sectional view of the transect as simulation domain when the aquifer has a uniform thickness of 3 m.

applied a coupled ground-surface water flow model to simulate periodic groundwater flow influenced by a sloping boundary, capillarity and vertical flows.

[4] Salinity investigation at the beach scale appears to have started in the last two decades. *Wrenn et al.* [1997] reported salinity measurements in two beaches in Maine, and were the first to note an inverted salinity distribution in the intertidal zone, whereby the saltwater overlays freshwater. *Robinson et al.* [1998] presented field observation of seasonal salinity variations in a coastal unconfined aquifer that depended on fresh groundwater discharge and surface water salinity/density gradient. *Boufadel* [2000] used experiments and numerical modeling using the MARUN model to analyze the salinity distribution in a laboratory beach. *Boufadel* [2000] provided guidelines for scaling up the results, and explained how the salinity distribution in tidally influenced beaches is characterized by an upper saline plume and the classical salt wedge. These two distinct saline plumes confined a freshwater discharge "tube", which pinches out near the low tide mark, contrasting with the traditional view of nearshore submarine groundwater discharge that is driven by density. *Mao et al.* [2006] reported saltwater intrusion and water table fluctuation in a tidally influenced sloping beach adjacent to a low-relief estuary through field investigation and numerical simulations. *Werner and Lockington* [2006] investigated salinity distribution and groundwater flow in an unconfined aquifer adjoining a partially penetrating, tidal estuary through numerical experiments. *Li et al.* [2008] investigated seawater-groundwater circulation in shallow beach aquifers, and developed a dimensionless formulation that allowed generalization of their results.

[5] All of the studies considered sandy beaches, and our study here deals with a gravel beach. Literatures of beach processes contain fewer studies of gravel beaches than study of sandy beaches [*Buscombe and Masselink*, 2006], possibly because sand beaches occur in parts of the world where their economic value to upland property and demand as a recreational asset are relatively greater. However, gravel beaches comprise a significant proportion of the world's coastlines [*Horn and Walton*, 2007; *Hayes et al.*, 2009]. Their functions as coastal defenses and natural habitats means that it is important to understand the processes occurring across the gravel beach face [*Buscombe and Masselink*, 2006]. Many investigations show that oil spills are potentially the most destructive pollution impacting gravel beaches [*Bodin*, 1988; *Owens et al.*, 2008; *Hayes et al.*, 2009].

[6] Here we present field measurements of water table and pore water salinities in a tidal gravel beach in Knight Island, Prince William Sound, Alaska, USA. The field results indicated the presence of two layers within the beach, and they were confirmed by numerical modeling using the code MARUN [*Boufadel et al.*, 1999a], a finite element code that allows one to simulate water flow and solute transport in both saturated and unsaturated zones of porous media taking into account the effect of water concentration on water density. The relationship between the water table behavior and the beach structure is discussed. The submarine groundwater discharge along the beach surface is analyzed over a spring-neap tide cycle. Comparisons with previous studies on homogeneous sandy beaches are made.

2. Field Description and Methodology

2.1. Field Site

[7] Measurements were conducted from 20 to 29 June 2008 in a cross-shore transect of the beach KN-114A located in Knight Island, Prince William Sound (147° 47′ 24.34" W, 60° 29′ 5.56" N; Figure 1a). The selected transect

Table 1. Surface Elevation and Thickness of the High-Permeable Surface Layer at Different Locations in the Transect[a]

Locations	x (m)	Surface Elevation z (m)	Thickness of Surface Layer (m)	Depth of Deepest Port (m)	Depth of Pit (m)
W1	0	4.95	0.8	0.83	1.02
P1	5.28	4.28	0.4	NA	NA
W2	10.56	3.61	0.4	0.62	0.81
W3	15.2	3.12	0.25	0.57	0.76
W4	19.66	2.51	0.1	0.69	0.88
W5	24.39	1.93	0.15	0.34	0.53
P2	28.47	1.68	0.2	NA	NA
P3	70.0	−0.86	0.2	NA	NA

[a]Points P1, P2, and P3 are reported because they represent a change in the surface geometry and/or the interface between layers. NA means not applicable.

was around 70 m long with an average beach slope of 10% in the intertidal area. The surface materials of the beach are made of pebbles, cobbles, and boulders, as noted visually in Figure 1b. Beneath the surface layer is a lower layer that comprises compacted grained sediments. The maximum tidal range during the study was 4.8 m (i.e., the tidal range during a spring tide).

[8] The beach was contaminated by the 1989 *Exxon Valdez* oil spills [*Neff et al.*, 1995]. But no oil residues were found in the transect that was established. The investigation herein would provide explanation on possible reasons for the disappearance of oil on this transect and its persistence at other locations within the sound [*Short et al.*, 2004, 2006; *Boehm et al.*, 2007; *Taylor and Reimer*, 2008].

2.2. Field Setup

[9] The transect consisted of five pits that were hand-dug because it was not possible to drive sensors into the beach due to the presence of boulders and the tightness of the sediments [*Taylor and Reimer*, 2008]. The depth of the pits ranged from 0.53 m to 1.02 m, as reported in Table 1. In each pit, a PVC pipe and a multiport sampling well were placed before refilling the pit. The PVC pipe was slotted over its whole length and contained at the bottom a self-logging pressure transducer (MiniDiver, Data Logger-DL501, Schlumberger) that provided the water pressure at 10 min intervals. A barometric (air) pressure sensor (BaroLogger, DL-500, Schlumberger) was used at the site and reported the barometric pressure at the same time interval.

[10] The multiport sampling wells were made of stainless steel and had 3 sampling ports spaced at 0.23 m intervals. They were labeled ports A, B and C from the bottom to the top. The elevations of the deepest port (Port A) for different wells are listed in Table 1. To prevent blockage by fine sediments to guarantee good hydraulic connection between the beach pore water and the water inside the well, the multiport well were wrapped with fine stainless steel screen. Each port was connected to the bottom of a stainless steel tube whose top was connected to a Luer lock three-way valve at the top of the well through a Tygon tubing.

[11] The observations of pore water pressure started on 20 June 2008, 12:35 A.M. (the initial time t = 0 for this paper), and the measurement durations differed with the locations (47~208 h). Measurements of the pore water pressure were used along with those of the barometric pressure and salinity to estimate the water table in each well. The salinities were measured at various depths using multiport wells placed at wells W1–W5. The initial time was at t = 20 h.

[12] Each pore water sample (approximately 100 mL) was collected by 60 mL Luer lock syringes and placed in 120 mL polyethylene bottles, and shipped to the laboratory at Temple University in Philadelphia, PA, for chemical analysis of chlorine concentration. The chlorine concentration of each sample was transformed into salinity based on the chlorine-salinity ratio of 19.4:35 [*Duxbury and Duxbury*, 2001]. Salinity data were obtained for a total of 76 samples by this method.

[13] As it was not possible to place a sensor at sea to allow measurement of the low tide, the full tidal fluctuation was estimated based on the observed data at Well 5 using the data during submergence of the beach at that location. This resulted in a time series of 749 data points at intervals of 10 min. Although there are 17 harmonic components for the tide [*Melchior*, 1964], we found that using five harmonic components was sufficient, namely:

$$H_{sea}(t) = H_0 + \sum_{i=1}^{5} A_i \cos(\omega_i t - \varphi_i) \tag{1}$$

where $H_{sea}(t)$ [L] is the tidal level and H_0 [L] is the mean sea level; the parameters A_i, ω_i and φ_i are the amplitude [L], tidal frequency [T^{-1}], and phase [rad] of ith tidal constituent, respectively. The subscript i represents each of the five harmonic components O_1, K_1, M_2, S_2 and N_2 (see Table 2) [*Merritt*, 2004].

[14] The least squares method was applied on equation (1) to obtain estimates of the parameters H_0, A_i, ω_i and φ_i, where H_0 equals to 2.60 m and the others were listed in Table 2. Figure 2 shows that the fit to the data at Well 5 (while submerged) was excellent. After the tidal level was determined, the elevation datum of the beach system was defined arbitrarily at the lowest tidal level (z = 0).

Table 2. Fitted Parameter Values for the Tide

i	A_i (m)	ω_i (1/hr)	φ_i (rad)	Explanation
1 (O_1)	−0.274	0.243	0.035	main lunar diurnal
2 (K_1)	−0.62	0.262	−0.581	lunar-solar diurnal
3 (M_2)	−1.331	0.506	4.541	main lunar semidiurnal
4 (S_2)	0.249	0.523	1.191	main solar semidiurnal
5 (N_2)	0.241	0.496	4.401	lunar elliptic

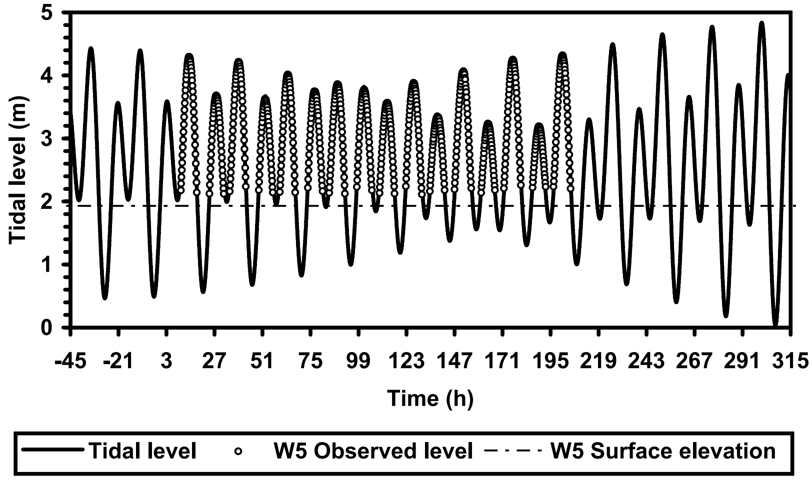

Figure 2. Tidal level during a spring-neap tidal cycle at the beach based on the water pressure observed at the well W5 when it was submerged. The initial time t = 0 h is 20 June 2008, 12:35 P.M.

[15] Rainfall occurred between 0:00 A.M. and 8:00 A.M., 23 June 2008, and the cumulative amount was measured at 1.5 cm, using a bucket rain gauge. This gives an average rainfall intensity of 4.5 cm/d (Figure 3a).

3. Numerical Implementation

3.1. Numerical Model

[16] The MARUN (MARine UNsaturated model) is a two-dimensional finite element model that can simulate water flow and solute transport in variably saturated porous media, taking into account the effects of salt concentration on fluid density and viscosity [*Boufadel et al.*, 1999a]. The governing equations of the MARUN model are presented in Appendix A. The MARUN model has been verified by reproducing previous well-known numerical results such as the Henry's problem of seawater intrusion [*Frind*, 1982; *Croucher and O'Sullivan*, 1995; *Boufadel et al.*, 1999a] and the Elder problem [*Elder*, 1967; *Boufadel et al.*, 1999b]. Other applications include tidal hydraulic [*Boufadel*, 2000; *Li et al.*, 2008], transient and steady seepage [*Boufadel et al.*, 1999c; *Naba et al.*, 2002] and nutrient application for bioremediation of oil spills on beaches [*Li et al.*, 2007; *Xia et al.*, 2010].

3.2. Boundary and Initial Conditions

[17] Figure 1c depicts the cross-shore domain of the simulation. The simulated beach has a length of 70 m and a uniform thickness of 3 m. At the saturated part of landward boundary of the domain, the observed water table and salinity at well W1 were used as the boundary conditions. No-flow boundary condition was assigned on the domain bottom and the boundaries of the unsaturated zone, which include the upper part of the landward boundary and the beach surface above sea level. The water pressure on the submerged beach surface was determined by the tidal seawater column above the beach surface, i.e., $\psi = \beta_{sea}[h_{sea}(t) - z]$, where β_{sea} is the density ratio of seawater to freshwater. Therefore, the sea boundary condition was moving with time. At each time step, the portion of the beach surface submerged by tide was updated by comparing the tidal level and beach surface elevation.

[18] The salinity boundary condition depended on the flow direction. At locations where seawater was entering the beach, the salt concentration was set equal to that of the sea (24.2 g/L). Otherwise, an outflow boundary condition was applied, where the water leaves the beach without a change in concentration with a zero dispersive flux. This approach is adopted in numerous works [e.g., *Galeati et al.*, 1992; *Boufadel*, 2000; *Michael et al.*, 2005; *Li et al.*, 2007].

[19] When digging pits, the original material of the lower layer was disturbed and replaced by loose, mixed materials from the surface and lower layers. This happened in spite of the careful effort to replace sediments as they were excavated. The permeability of the materials of the lower layer in the pit was therefore enhanced dramatically. This "pit effect" was accounted for in model calibration by viewing the pit as a zone the permeability of which is comparable to that of the surface layer. Each pit was 0.4~0.6 m in diameter at the top narrowing down to 0.2~0.3 m at the bottom. The bottom of the pit was 0.19 m lower than the deepest sampling port (i.e., port A, Table 1).

[20] The initial condition was a hydrostatic state at low tide with a sharp freshwater-seawater interface as given by the Ghyben-Herzberg approximation [*Bear*, 1988], and several spring-neap tidal cycles (approximately 150 days) were run to obtain the quasi-steady state numerical solution, such that the "signature" of the initial condition disappeared.

3.3. Numerical Implementation

[21] The domain was discretized using a mesh consisting of 675 nodes in the horizontal direction and 31 nodes in the vertical direction, resulting in a total of 20,925 nodes, and 40,440 triangular elements. The mesh resolution was ~0.1 m.

[22] The upper limit of the time step was set such that the grid Courant number remained less than 0.95 (The courant number is defined as $C_r = \frac{v \Delta t}{\Delta l}$, where "v" is the Darcy velocity, Δl is the maximum of Δx and Δz of the mesh). The convergence criterion of the Picard iteration for solving the nonlinear groundwater flow equation was 10^{-5} m. The

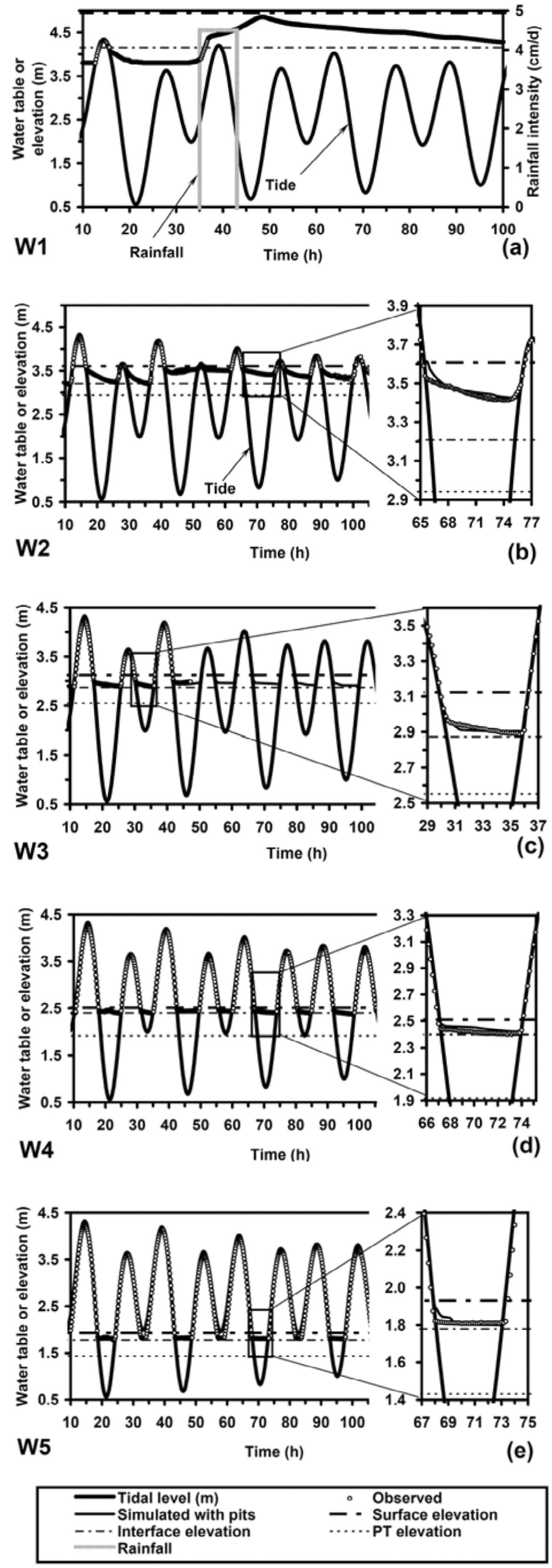

seepage module in MARUN [*Naba et al.*, 2002] was disabled as no seepage face was observed during the study.

4. Results

4.1. Water Table

[23] Figure 3 reports the variations of the observed and simulated water table with time at wells W1-W5. The observed water table landward of the beach (W1, Figure 3a) was almost constant before the time t = 35 hours. It increased abruptly at around t = 35 hours due to rainfall that occurred during the period of 35~43 h. It reached then the maximum height of 4.9 m at t = 48 hours, which has a time lag of 5 h relative to the rainfall, and then decreased with time. The water level at W1 was higher than the tidal level most of the time, which suggests that the beach was consistently filled from inland freshwater recharge. This is a common situation observed in many studies [e.g., *Ullman et al.*, 2003; *Destouni and Prieto*, 2003].

[24] Note in Figure 3b that due to the rainfall that occurred during 35–40 h, the water table at W2 at low tides after t = 40 h was higher than that before t = 40 h. The effect of rainfall on the water table at W3 (Figure 3c) during low tides seems to be present only for the two consecutive tides (between 48 h and 60 h). The rainfall has no apparent effect on the water table at W4 and W5, indicating that the water table at these wells was chiefly affected by the tide. However, the salinity at these wells (discussed in section 4.2) was still dependent on rainfall-runoff at W1.

[25] Figure 3b shows that when the observed water level at W2 fell below the beach surface, it kept falling at the same speed as the falling tide for a certain depth, and then became almost constant until subsequent flood tide. The same behavior is noted for sensors W3 (Figure 3c), W4 (Figure 3d), and W5 (Figure 3e). This behavior of water table variation indicates that the beach can be viewed as consisting of two layers: A surface layer with hydraulic conductivity that is so high such that the water table within it drops unhindered (i.e., closely following the tide), and a lower layer whose hydraulic conductivity is so low such that the water within it practically does not fall off with time (or falls very slowly with time).

4.2. Salinity

[26] The average salinity in the samples collected from the seawater adjacent to the beach was 24.2 g/L, which is close to values reported by *Coyle and Pinchuk* [2005], where they reported that the salinity of shallow seawater varies seasonally and is 28.8 ± 0.8 g/L during the beginning of July in Prince William Sound.

[27] Figure 4 shows the observed and simulated salinity variations with time in the 5 wells W1–W5. Results from

Figure 3. Observed (circles) and simulated (solid lines) water table at wells (a) W1, (b) W2, (c) W3, (d) W4, and (e) W5. The solid lines are simulation results with pits included. The tidal level and the elevations of the beach surface, of the interface between the surface and lower layers, and of the PTs (pressure transducers) installed at these observation wells are also shown to indicate the submersion period.

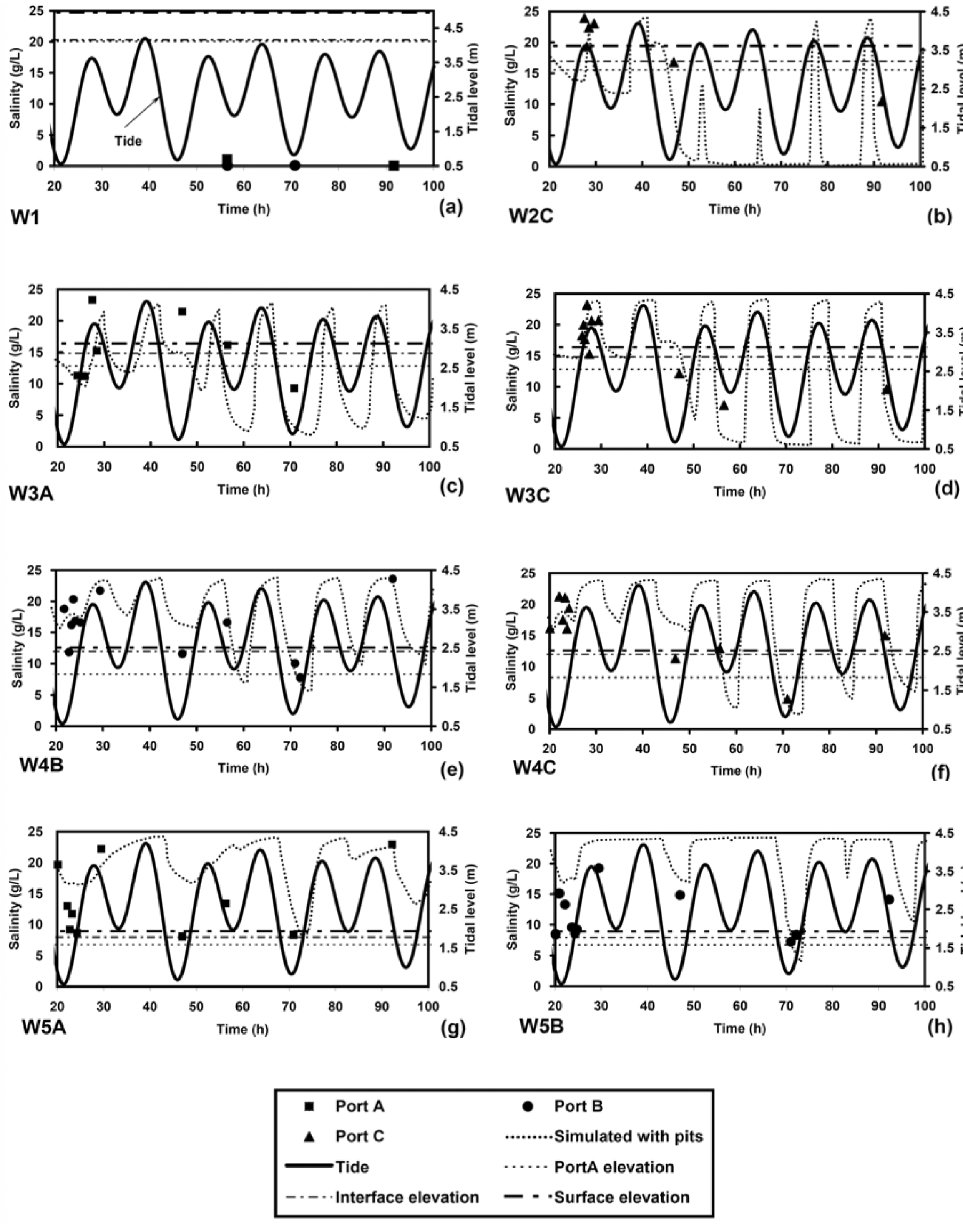

Figure 4. Observed (symbols) and simulated (dotted lines) salinities of the pore water at ports of W1, W2, W3, W4, and W5. The dotted lines are simulation results with pits included. The tidal level and the elevations of the beach surface, of the interface between the surface and the lower layers, and of the sampling port A installed at these observation wells are also shown.

some ports were not available due to clogging. The observed salinity at different locations (Ports A, B and C) of the wells W2–W5 (Figures 4b–4h) fluctuated with the tidal level dramatically, reaching 24.0 g/L at high tides and decreasing to 5.0 g/L at low tides. Figure 4b shows the variation of pore water salinity with time at Port C of W2, which is located in the surface layer. The observed salinity fluctuated with tide, reaching the maximum of 24.0 g/L at $t = 28$ hours. Figure 4c and Figure 4d report the variation of pore water salinity with time at Ports A and C of W3, respectively. The effect of

Table 3. Model Parameters and Their Values Used in the Numerical Simulations

Parameter	Definition	Unit	Value
α	capillary fringe parameter of the *van Genuchten* [1980] model	m^{-1}	40.0
n	sand grain size distribution parameter of the *van Genuchten* [1980] model	-	7.0
K	hydraulic conductivity for saturated freshwater	m/s	10^{-3} and 10^{-2} (surface layer) 10^{-5} (lower layer)
ϕ	saturated water content	m^3/m^3	0.30
S_r	residual water content	m^3/m^3	0.01
S_s	specific storativity	m	10^{-5}
β_{sea}	density ratio of the seawater to freshwater	-	1.02
α_L	longitudinal dispersivity	m	0.1
α_T	transverse dispersivity	m	0.005
τD_m	molecular diffusion coefficient in porous media	m^2/s	10^{-9}

rainfall is apparent through the decrease of salinity at both ports A and C during low tides between 48 h and 75 h. This was captured by the model.

[28] Figure 4e and Figure 4f report the variation of pore water salinity with time at Ports B and C of W4, respectively. The salinity during low tides decreased from 15.0 g/L before $t = 56$ h to 5.0 g/L after $t = 56$ h. The lowest values are noted during the spring tide around 70 h. Figure 4g and Figure 4h show the variation of pore water salinity with time at Ports A and B of W5, respectively.

[29] Note that the rainfall-runoff caused the abrupt water table rising at W1 around $t = 36$ h (Figure 3a), which can be regarded as a fresh groundwater flood from inland. Due to the seaward movement of the front of the fresh groundwater flood, two stages of salinity variation formed clearly at each location. The first is the "high-salinity" stage before the freshwater front arrived. The second is the "low-salinity" stage when and after the freshwater front arrived. The duration of the high-salinity stage increased significantly as the well location moved seaward, from about 50 h at W3, to 73 h at W5. This is because the traveling time required for the fresh groundwater flood from W1 to the other wells increased seaward.

[30] Figure 4 also shows that the salinities during extreme low tides were smaller than those during other low tides; this is because more freshwater could arrive at the observation wells during the extreme low tides than during other low tides.

4.3. Model Validation

[31] Four major parameter groups were estimated: (1) the layer thickness, (2) the hydraulic conductivities of the two layers, (3) capillarity parameters, and (4) dispersivities. These parameters are reported in Table 3.

[32] The thickness of the surface layer at different locations was estimated based on field inspection and model calibration, especially of the water module within MARUN. Table 1 reports that the thickness decreased going seaward from 0.8 m at $x = 0.0$ m to 0.1 m at $x = 20$ m and then increased slightly to 0.2 m at $x = 28$ m. Seaward of that location, the thickness was assumed to remain at 0.2 m. Although we do not have information to confirm this assumption, it should not affect beach hydraulics landward of $x = 30$ m.

[33] The saturated hydraulic conductivity of the layers was determined mainly based on model calibration. For the surface layer, the hydraulic conductivity was found to be around 10^{-3} m/s for 0 m < x < 12 m, and 10^{-2} m/s for 12 m < x < 70 m, where x is the seaward horizontal distance from W1. The hydraulic conductivity of the lower layer was found to be 10^{-5} m/s.

[34] Sediment samples taken at three or four depths in each pit were used to estimate the permeability of each zone using the Kozeny-Carmen equation [*Carrier*, 2003]. There was a total of 19 sediment samples, 9 of them from the surface layer (5 for 0 m < x < 12 m and 4 for 12 m < x < 70 m) and 10 from the lower layer. The grain size distribution provided the Effective Diameter [*Carrier*, 2003], which was used along with the measured porosity in the lab to compute the hydraulic conductivity of each sample. The hydraulic conductivity K was found using the Kozeny-Carman equation [*Carrier*, 2003], to be 0.008 m/s (0 m < x < 12 m) and 0.003 m/s (12 m < x < 70 m) for the average grain size distribution of sediment samples from surface layer. It was found to be 0.0025 m/s for the sediments of the lower layer.

[35] The laboratory measured K value is larger than that obtained by calibration of the model for the lower layer, which is due to the fact that the sediments of the lower layer were tightly compact in the field, and they became loose after extraction. For the surface layer, the laboratory-measured K value has the same magnitude of that obtained by calibration of the model, because the sediments are relatively loose as a result of high water flow through them (waves, runoff) and the small pressure of the overburden in the field.

[36] As one notes in Figure 3, the difference between the simulated and observed water table was less than 0.05 m in most cases. This reflects a good agreement between simulated and observed results considering the uncertainty in beach characteristics and the large tidal range of ~4.8 m.

[37] The simulated salinity at W2 tended to zero at low tides after $t = 55$ hours, reflecting dilution by freshwater induced from rainfall-runoff. This is also supported by the low observed salinity at $t = 92$ h.

[38] In Figures 4e and 4f, the model provided a good match with the data, especially after $t = 56$ h. Note the good agreement, for example, during the low tide around $t = 70$ h. The simulated pore water salinity at Ports A and Ports B of W5 are reported in Figure 4g and Figure 4h, respectively. The simulated salinities were, in general, larger than the observed ones, especially at Port A during 40–60 h. This might be due to local heterogeneity of the beach sediments near W5. Despite of this, the simulated results captured the main fluctuating trend of the salinity with time, particularly the low salinity observed around $t = 70$ h.

Table 4. Model Setup for Numerical Simulations[a]

Model	Hydraulic Conductivity (m/s) Surface Layer Zone 1	Surface Layer Zone 2	Lower Layer	Pits Zone 1	Pits Zone 2	Longitudinal Dispersivity (m)	Transverse Dispersivity (m)
1	10^{-3}	10^{-2}	10^{-5}	10^{-3}	10^{-2}	0.1	0.005
2	10^{-3}	10^{-2}	10^{-4}	10^{-3}	10^{-2}	0.1	0.005
3	10^{-3}	10^{-2}	10^{-6}	10^{-3}	10^{-2}	0.1	0.005
4	10^{-3}	10^{-2}	10^{-5}	10^{-3}	10^{-2}	0.5	0.1
5	10^{-3}	10^{-2}	10^{-5}	5×10^{-3}	5×10^{-2}	0.1	0.005
6	10^{-3}	10^{-2}	10^{-5}	5×10^{-4}	5×10^{-3}	0.1	0.005
7	5×10^{-3}	5×10^{-2}	10^{-5}	5×10^{-3}	5×10^{-2}	0.1	0.005
8	5×10^{-4}	5×10^{-3}	10^{-5}	5×10^{-4}	5×10^{-3}	0.1	0.005

[a]Zone 1 and zone 2 denote the zones of 0 m < x < 12 m and 12 m < x < 70 m, respectively, where x is the seaward horizontal distance from W1.

4.4. Sensitivity Analysis

[39] Seven numerical models were simulated for sensitivity analysis to assess the effect of the hydraulic conductivities, dispersivities, and the parameterization of the pits on the results (see Table 4). In each simulation, only the value of the model parameter for sensitivity analysis was changed and all the other parameters were fixed as listed in Table 3.

[40] For brevity of the main manuscript, the sensitivity of pit effect is reported in the Appendix B (Model 5 and Model 6).

4.4.1. Effect of Hydraulic Conductivity

[41] The sensitivity of the results to the value of the hydraulic conductivity of the surface layer is reported in Appendix B (Model 7 and Model 8) for brevity of the main article, and because the laboratory results provided K values that are comparable to the calibrated K values. We discuss next the sensitivity of the results to the hydraulic conductivity of the lower layer.

[42] When the hydraulic conductivity of the lower layer was increased from 10^{-5} m/s (Model 1) to 10^{-4} m/s (Model 2), the simulated water table at wells W2, W3 and W5 was lower than that of Model 1, especially at W3 (Figure 5). The water table simulated by Model 2 was close to that of Model 1 at wells W4 (not shown here).

[43] The salinities simulated by Model 2 were consistently lower than the observed ones, but those of Model 1 were reasonably close to the observations (Figure 6), especially at Port A of W3 (Figure 6a), and Port B of W4 (Figure 6b). For example, for Port A of W3 (Figure 6a) one notes that at t = 25 hours, the error between the simulated salinity by Model 2 and observed one is 7.5 g/L (a relative error 67%). On the other hand, the error between the simulated salinity by Model 1 and the observed one is only about 1.0 g/L (a relative error of 10%). These results indicated that the hydraulic conductivity of the lower layer of Model 2 is high and provide a large flow of freshwater that overdiluted the salinity of the beach pore water.

[44] When the hydraulic conductivity of the lower layer was decreased from 10^{-5} m/s (Model 1) to 10^{-6} m/s (Model 3), the simulated water table was very close to that the observed and that obtained from Model 1. For this reason, it is not shown. Thus, one is led to conclude that decreasing the hydraulic conductivity of the lower layer had no effects on the water table at wells W2–W5. However, the difference between Model 3 and Model 1 (and the observed data) was large for the salinity. Figure 7 shows that the match between

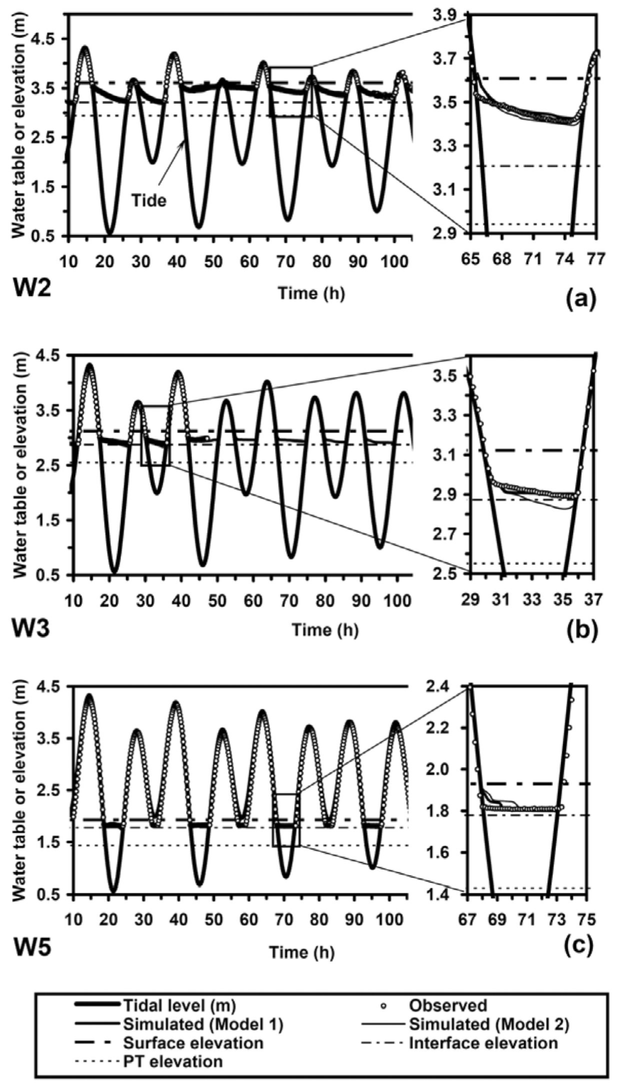

Figure 5. The water table at wells W2, W3, and W5 when the hydraulic conductivity of the lower layer was increased from 10^{-5} m/s (Model 1) to 10^{-4} m/s (Model 2). Symbols represent observations, and solid lines represent the simulations. The thick solid lines are simulation results of Model 1, and the thin solid lines are simulation results of Model 2. The tidal level and the elevations of the beach surface, of the interface between the surface and the lower layers, and of the PTs (pressure transducers) installed at these observation wells are also shown to indicate the submersion period.

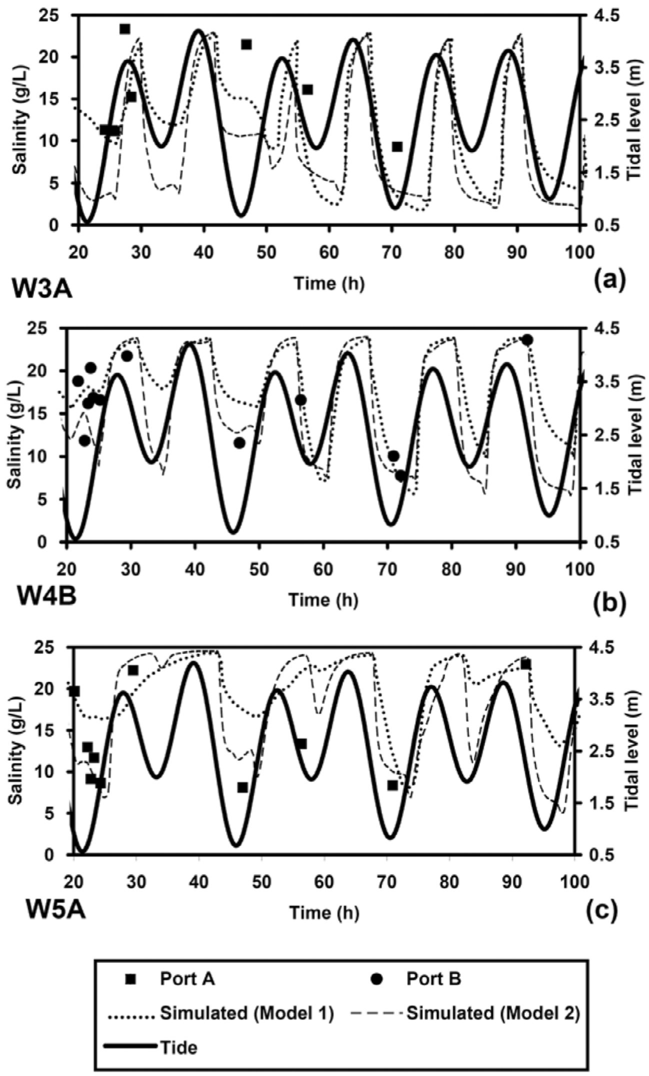

Figure 6. Salinity of the pore water at ports of W3, W4, and W5 when the hydraulic conductivity of the lower layer was increased from 10^{-5} m/s (Model 1) to 10^{-4} m/s (Model 2). Symbols represent observations, and dotted and dashed lines represent the simulations. The dotted lines are simulation results of Model 1, and the dashed lines are simulation results of Model 2. The tidal level is also shown.

the observed and simulated salinities of Model 3 became worse than that of Model 1. The salinity simulated by Model 3 was higher than the observed ones, particularly during falling tides and at low tide at Port A of W3 (Figure 7a), Ports B of W4 (Figure 7b) and Port A of W5 (Figure 7c). These results demonstrate that the hydraulic conductivity of the lower layer of Model 3 is too low to provide enough fresh water at low tide for diluting the pore water. Therefore, the hydraulic conductivity of Model 1 is the optimal one.

4.4.2. Effect of Dispersion

[45] Quantifying dispersion is crucial for understanding the mixing between water masses in a beach environment. Studies on dispersivity were based on flow through heterogeneous aquifers [*Gelhar and Axness*, 1983; *Neuman*, 1990; *Rajaram and Gelhar*, 1993], and suggest that the macrodispersivity (or field dispersivity) should be around 5% to 10% of the domain length. This has led some researchers dealing with tidally influenced beaches to use relatively large values in numerical simulations. The field-scale dispersivity depends on the traveled path and while such paths are practically horizontal and constant with time in inland aquifers, they are highly dynamic and convoluted in tidally influenced beaches; beaches fill from the sea during high tides and drain during low tides. The circulation cell was noted in numerous works [*Boufadel*, 2000; *Ataie-Ashtiani et al.*, 2001; *Boufadel et al.*, 2006; *Brovelli et al.*, 2007]. Therefore, the domain dispersivity, should be based on some integrated measure of paths of various lengths, and it should be always smaller than the dispersivity obtained by assuming water traveling the whole length of the beach.

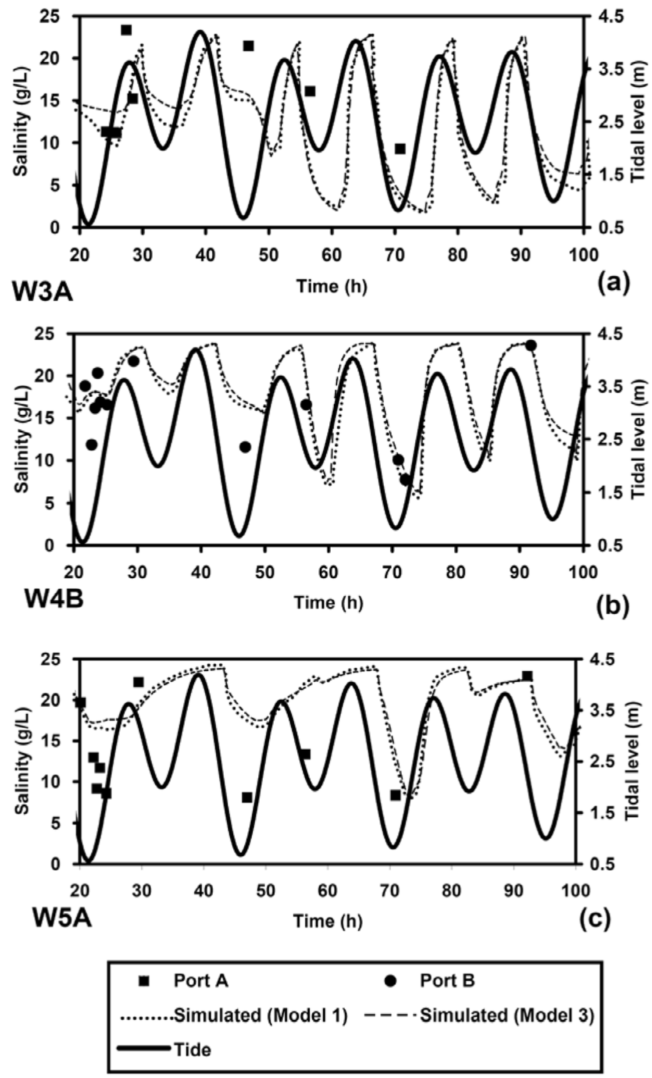

Figure 7. Salinity of the pore water at ports of W3, W4, and W5 when the hydraulic conductivity of the lower layer was decreased from 10^{-5} m/s (Model 1) to 10^{-6} m/s (Model 3). Symbols represent observations, and dotted and dashed lines represent the simulations. The dotted lines are simulation results of Model 1, and the dashed lines are simulation results of Model 3. The tidal level is also shown.

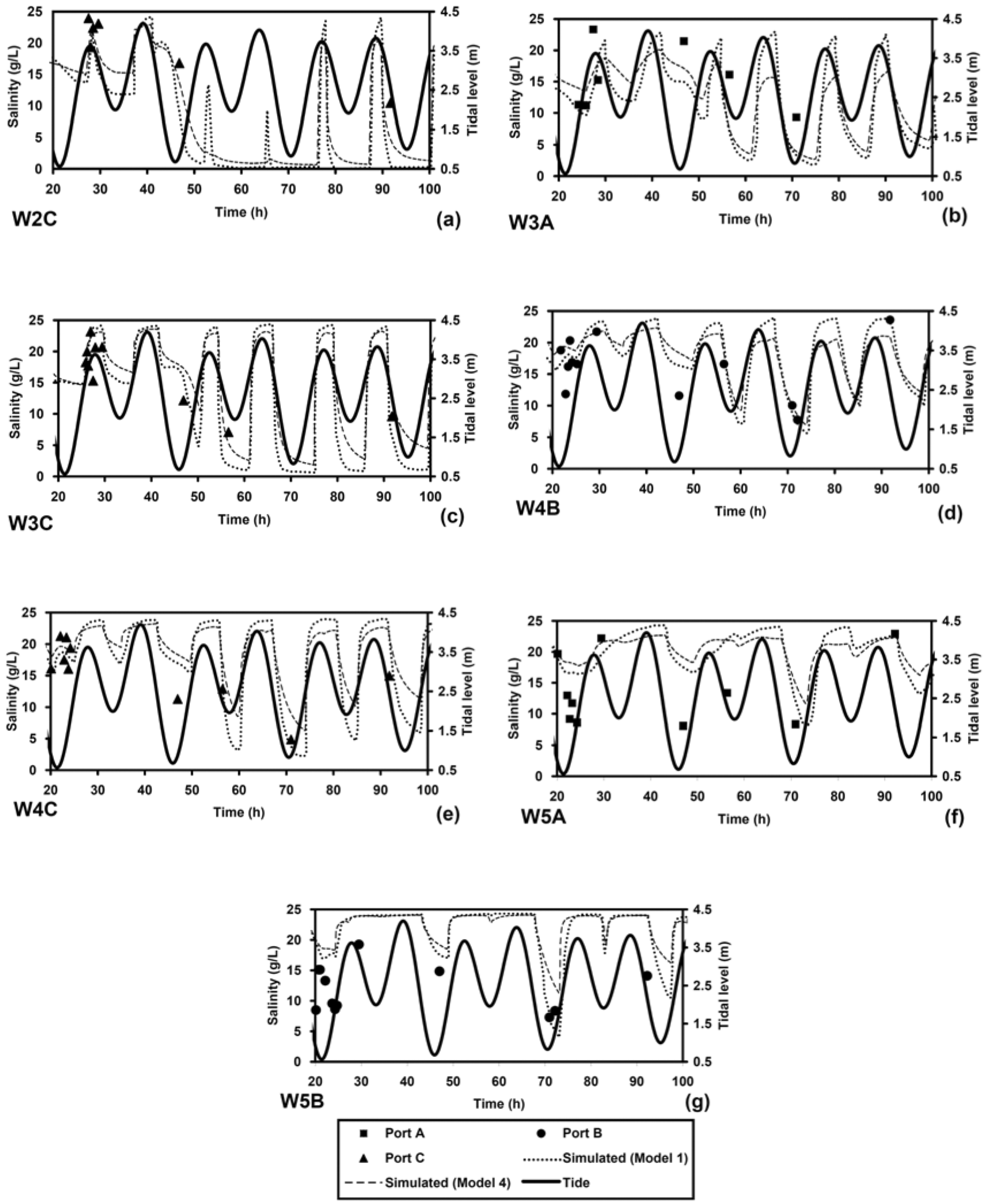

Figure 8. Salinity of the pore water at ports of W2, W3, W4, and W5 when the longitudinal dispersivity was increased from 0.1 m (Model 1) to 0.5 m (Model 4) and the transverse dispersivity was increased from 0.005 m (Model 1) to 0.1 m (Model 4). Symbols represent observations, and dotted and dashed lines represent the simulations. The dotted lines are simulation results of Model 1, and the dashed lines are simulation results of Model 4. The tidal level is also shown.

[46] We found by calibration that the longitudinal dispersivity α_L is 0.1 m (Model 1) supporting our argument above (i.e., α_L much smaller than 5% of the domain length, which would be 3.5 m). The transverse dispersivity α_T was found to be 0.005 m. When these values were increased to α_L = 0.5 m and α_T = 0.1 m (Model 4), the match between the observed and simulated salinities became worse than those of Model 1 at most of the ports (Figure 8). The salinity simulated by Model 4 was generally high near low tides (e.g., W5B). The difference was not too large, however, suggesting that intermediate dispersivity values between Model 1 and Model 4 would still be acceptable overall.

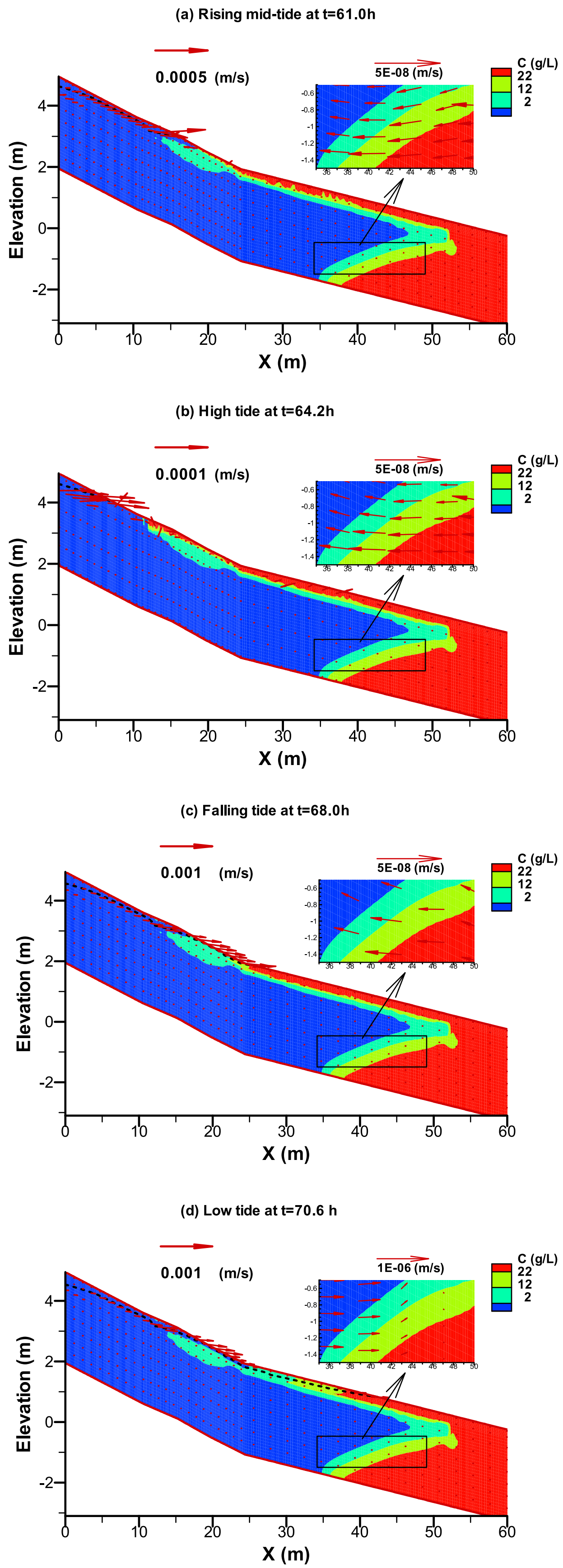

Figure 9. Spatial salinity distribution and groundwater table for (a) rising midtide, (b) high tide, (c) falling midtide (d), and low tide. Banded colors are contours of salinity of the pore water, and black dashed lines represent water table. Vectors were used to indicate the velocity direction and magnitude.

4.5. Evaluation of Exchange

[47] In order to investigate the groundwater flow and salt transport in the intact sediments of the tidal beach without artificial perturbation, simulations that excluded the pit effects were conducted after model calibrations. The model parameters identified using the observed water table and salinity in previous sections were used in the simulations.

[48] Figure 9 shows the water table, velocity vectors, and contours of salinity distribution at rising midtide (t = 61.0 h), high tide (t = 64.2 h), falling midtide (t = 68.0 h), and low tide (t = 70.6 h). When tides rose from the midtide to high tide, the salt plume spread landward in the top section of the beach along the surface layer (Figures 9a and 9b). When tides fell from the midtide to low tide, the salt plume in the top section of the beach withdrew seaward (Figures 9c and 9d). Figure 9 indicates that the salinity generally decreased with depth until it reached a zero value (freshwater). A saltwater wedge formed near the low tide line (around x = 45 m). The two parts of the salt plume were produced by different mechanisms: the upper part was due to salt transport associated with tidally driven seawater-groundwater circulation, and the lower part (wedge) was due to saltwater intrusion, a situation similar to those observed by *Boufadel* [2000] and *Li et al.* [2008].

[49] The salinity in the salt wedge seaward of the low tide line was almost unchanged with the tide in comparison with the salt plume in the surface layer of the intertidal zone, which varied closely with the tide. This was noted in previous studies in homogeneous beaches [*Ataie-Ashtiani et al.*, 1999; *Boufadel*, 2000; *Li et al.*, 2008]. In addition, the freshwater discharge "tube" between the upper saline plume and salt wedge first observed by *Boufadel* [2000] did not appear here, probably due to the two-layered structure of the beach as explained next.

[50] The salt from the sea disperses landward and is opposed by seaward convection of freshwater. Due to the permeability contrasts, water propagating seaward in both layers tends to exit the beach through the surface layer, especially landward of the slope break at x = 25 m (note the large velocity vectors in Figure 9d). This implies that the freshwater flow reaching the interface at 40 m is considerably reduced and is not capable of clearing of path "the tube" before the tide rises again. Thus, the salinity distribution in this gravel beach is unlike studies in sandy beaches [*Boufadel*, 2000; *Robinson et al.*, 1998]. A similar salinity distribution was observed in a two-layered beach in Prince William Sound [*Li and Boufadel*, 2010].

[51] Figure 10 reports the Darcy velocity distribution within the beach averaged over the observation period (208 h). The bulk of the freshwater in the beach comes from the landward side W1, and the flow direction is seaward. The velocity in the surface layer is much higher than that in the lower layer due to the permeability difference between the two layers. Note the decrease in velocity mag-

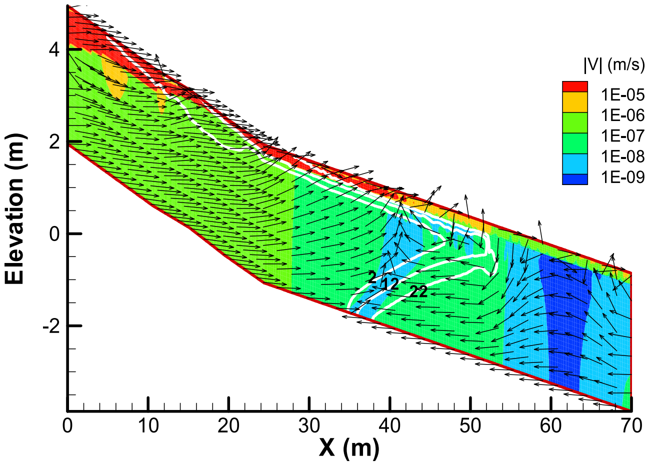

Figure 10. Average pore water velocity and salinity in the transect calculated over the observation period (208 h). Vectors with uniform length were used to indicate the velocity direction but not its magnitude. The three solid white curves are contours of the pore water salinity. They are 2 g/L, 12 g/L, and 22 g/L and are to be read from bottom left to top right.

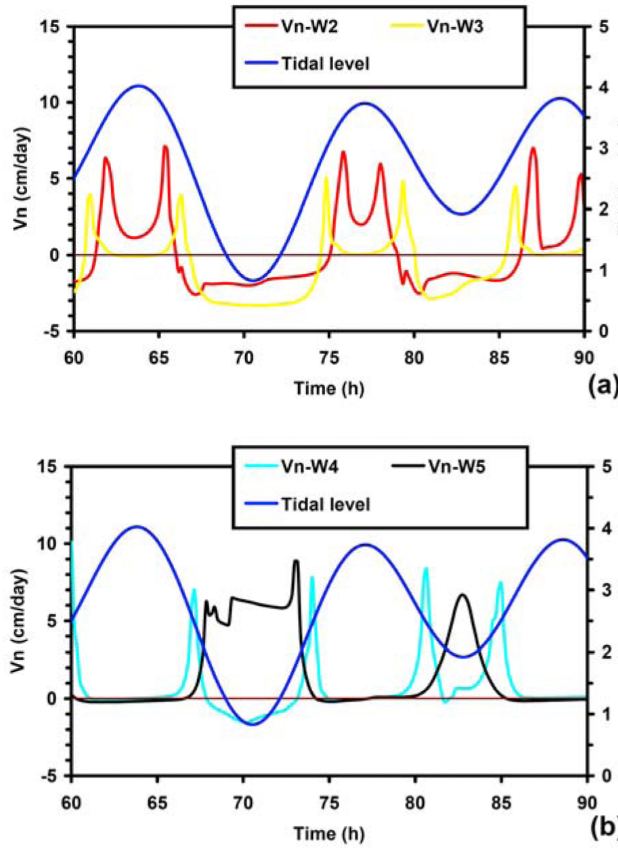

Figure 11. Simulated pore water normal velocities at four different locations in the transect during a spring tidal cycle and a neap tidal cycle. The normal velocity is defined as the velocity normal to the interface of the surface and lower layers. The four locations were chosen as the points 0.1 m below the two layers' interface at wells (a) W2 and W3 and (b) W4 and W5.

nitude at the saltwater interface (approximately x = 40 m). Note also the landward pointing velocity at x > 40 m. In particular at x = 45 m at 0.40 m below the beach surface (the interface of the two layers is 0.20 m below the beach surface) there are two velocity vectors pointing landward. Thus, salt dispersion in the lower layer is acting to close in on the freshwater tube. Interestingly, the velocity vectors at locations in the surface layer, are pointing seaward reflecting the fact that seaward convection is large in the surface layer. One could also note the circulation of seawater near the low tide.

[52] Figure 11 shows time series of pore water velocity at location 0.1 m below the interface of wells W2–W5. For W2 and W3 (Figure 11a), focusing on the period between t = 60 h and t = 70 h, one notes: as the tide rises, the layer fills from below causing water coming from the land side to rise out of the lower layer (t = 61 h for W3 and t = 62 h for W2). The flow decreases in magnitude as the tide rises until it reaches a minimum at high tide. The outward flow from the lower layer at W2 and W3 increases again (t = 65 h for W2 and t = 67 h for W3) almost at the same tidal elevation that caused the earlier peaks. As the tide level drops, water begins entering the lower layer while being supplied through the high-permeability surface layer.

[53] In order to estimate the tide-induced submarine groundwater discharge (SGD) across the beach-sea interface of the intact beach, the outflow and inflow rates of water along the beach face averaged over a spring-neap tide cycle were computed. Figure 12 shows the percentage of inflow rate and outflow rate (volume of seawater entering or flowing through the beach domain in unit length of the beach surface in the cross-shore direction and unit length in the long-shore direction per day). They can reach their maximum ratio, 19% of total rates in the middle intertidal zone (tidal height interval of 1.8~2.3 m). From Figure 12, one can conclude that the major portion of seawater-groundwater circulation occurred in the intertidal zone. The total submarine groundwater discharge (SGD) was 10.24 m^3 d^{-1} m^{-1} (by integrating the outflow rate along the whole beach face). In addition, the total inland freshwater recharge from the left boundary was 1.48 m^3 d^{-1} m^{-1}. Therefore, the net discharge is 8.76 m^3 d^{-1} m^{-1}, which is given by the

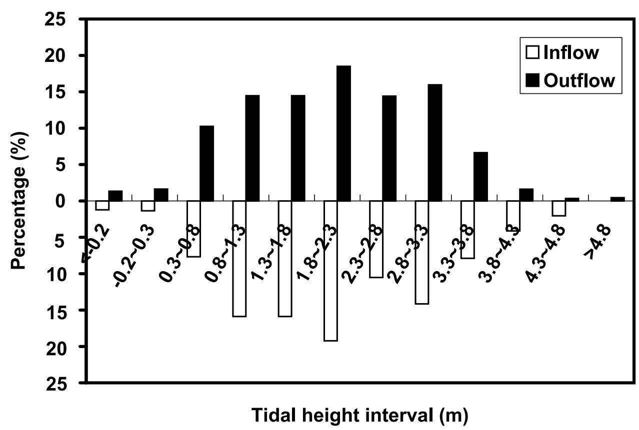

Figure 12. Distributions of the inflow and outflow rate (percentage) across the beach-sea interface versus tidal height intervals during a spring-neap tidal cycle.

difference between the total SGD and freshwater discharge. The fresh groundwater discharge constituted 14.4% of the total SGD over the spring-neap period, which is higher than previous studies [e.g., *Younger*, 1996; *Church*, 1996], where they stated that 4% SGD is from inland freshwater recharge. Our large value is most likely due to the high permeability of the surface layer.

[54] *Michael et al.* [2005] considered the effects of seasonal variation of inland recharge on SGD and obtained an estimation of SGD ~7.0 m^3 d^{-1} m^{-1} through a coastal zone at Waquoit Bay, Massachusetts, USA. *Robinson et al.* [2007] considered seawater-groundwater exchange along the aquifer-ocean interface in a sandy beach aquifer. The tidal range varied from approximately 2.2 m at the spring tide to 1.1 m at the neap tide. The total SGD was estimated at 5.1 m^3 d^{-1} m^{-1} at spring tide and 4.1 m^3 d^{-1} m^{-1} at neap tide. Compared with the SGD in previous works [*Michael et al.*, 2005; *Robinson et al.*, 2007], our SGD is larger than theirs, which is probably due to the large tidal range of 4.8 m in our beach and the very permeable surface layer [*Destouni and Prieto*, 2003; *Li et al.*, 2008].

5. Effect on Oil Persistence

[55] This beach was heavily polluted by the *Exxon Valdez* oil spill in 1989. Therefore, the question that emerges is why this beach is relatively "clean" while a beach 100 m south of it, KN114A remains heavily polluted [*Short et al.*, 2004, 2006; *Taylor and Reimer*, 2008]. We believe this to be related to the elevation of the water table with respect to the interface of the two layers. First, it is important to discuss the mechanisms of oil infiltration into the beach; during the initial oiling, the rapid fall of the water table with the falling tide within the highly permeable surface layer allowed oil stranded on the beach surface to penetrate the interstices of the surface layer, sheltering it from continued weathering if it was remaining on the beach surface. Therefore, that oil, most likely kept its initial low viscosity and high fluidity [see also *Short et al.*, 2006]. In this regard, the surface layer acted as reservoir for the slow, continuous filling the lower layer whenever the water table dropped below the interface of the two layers. In the beach studied in this paper, the water table remained above the interface of the two layers due to variety of reasons, such as the large groundwater flow and/or a deep surface layer. Therefore, it is likely that oil remained only in the surface layer, and got washed out due to the vigorous level of cleaning and/or the passing of 20 years. It is also possible that oil trapped in the surface layer biodegraded due to the presence of sufficient oxygen. The nutrient concentration in the surface layer is small [*Bragg et al.*, 1994; *Atlas and Bragg*, 2009], but one would expect considerable biodegradation after 20 years if sufficient oxygen is present [see *Venosa and Zhu*, 2003].

6. Conclusions

[56] This paper investigated the interaction of groundwater and seawater in a tidally influenced gravel beach. Field observations of water table, pore water salinity were performed. The two-dimensional finite element model MARUN [*Boufadel et al.*, 1999a] was used to simulate observed water table and salinity. Based on field observations and model calibrations, a two-layered beach structure was identified which is characterized by a high-permeability surface layer underlain by a low-permeability lower layer.

[57] The observed data and numerical simulations demonstrated the following important facts:

[58] 1. The behavior of water table variation indicates that the beach needs to be viewed as made up of two layers. The salt wedge seaward of the low tide line was almost invariant in comparison with the strong fluctuations of the salinity plume in the surface layer of the intertidal zone.

[59] 2. The presence of the two layers prevented the presence of a freshwater discharge "tube" between the upper saline plume and salt wedge. This is in contrast with the previous works where freshwater discharge tube were observed [*Boufadel*, 2000; *Robinson et al.*, 2006]. The tide-induced submarine groundwater discharge (SGD) was estimated at 9 m^3 d^{-1} m^{-1}. This is a large value that is probably due to the large tidal range of ~4.8 m and the very permeable surface layer. The freshwater-seawater dynamics revealed here may provide new insights into the complexity, intensity and time scales of mixing between fresh groundwater and seawater in tidal beaches.

[60] 3. A sensitivity analysis revealed that the estimated parameters are well determined, especially when one attempts to match both the observed water table and salinity.

[61] 4. The simulated water table of the beach is higher than the interface between the surface and lower layers, which prevented *Exxon Valdez* oil from penetrating into the lower layer in 1989.

Appendix A

[62] The water flow equation for homogeneous, isotropic two-dimensional domains can be written as [*Boufadel et al.*, 1999a; *Boufadel*, 2000]:

$$\beta\phi\frac{\partial S}{\partial t} + \beta S_0 S\frac{\partial \psi}{\partial t} + \phi S\frac{\partial \beta}{\partial t} = \frac{\partial}{\partial x}\left(\beta\delta k_r K_0\frac{\partial \psi}{\partial x}\right) + \frac{\partial}{\partial z}\left[\beta\delta k_r K_0\left(\frac{\partial \psi}{\partial z} + \beta\right)\right], \quad \text{(A1)}$$

where ψ [L] is the pressure head, ϕ [-] is the porosity, S [-] is the degree of water saturation (fraction of pore volume occupied by water), S_0 [L^{-1}] is the specific storage, K_0 [LT^{-1}] is the saturated hydraulic conductivity for freshwater (constant), k_r is the relative permeability, β is the density ratio defined as:

$$\beta = \frac{\rho}{\rho_0} = 1 + \varepsilon\ c \geq 1, \quad \text{(A2)}$$

where ρ [ML^{-3}] is the density of the beach pore water, ρ_0 = 998.2 kg m^{-3} is the fresh water density at 20°C, ε is a fitting parameter and equals 7.63 × 10^{-4} m^3 kg^{-1}; c is the salt concentration [ML^{-3}] of the beach pore water, δ is the dynamic viscosity ratio defined by *Boufadel et al.* [1999a] as:

$$\delta = \frac{\mu_0}{\mu} = 1 - \xi\ c \leq 1, \quad \text{(A3)}$$

where μ [ML^{-3}T^{-1}] is the dynamic viscosity of the beach pore water, $\mu_0 = 0.001$ kgm^{-3}s^{-1} is the dynamic viscosity of the fresh water at 20°C, and ξ is a constant equal to 1.566×10^{-3} m^{3}kg^{-1}.

[63] The soil moisture ratio and the relative permeability are correlated by the *van Genuchten* [1980] model:

$$\text{For } \psi \geq 0: S = 1.0, k_r = 1, \tag{A4}$$

$$\text{For } \psi < 0,\ k_r = \sqrt{S_e}\left[1 - \left(1 - S_e^{1/m}\right)^m\right]^2, \tag{A5}$$

where S_e is the effective saturation ratio given by:

$$S_e = \frac{S - S_r}{1 - S_r} = \left[\frac{1}{1 + (\alpha \mid \psi \mid)^n}\right]^m, \tag{A6}$$

where $m = 1 - \frac{1}{n}$, S_r is the residual saturation ratio, α [L^{-1}] represents the characteristic pore size of the beach soil, and higher α values imply a coarser material. The inverse of α provides an estimate of the capillary fringe (zone of considerable moisture above the water table). The term n represents the uniformity of the pores and higher values of n imply a more uniform pore size distribution [*van Genuchten*, 1980].

[64] The solute transport equation is the well-known convection-dispersion equation. In the absence of source/sink term, it can be written as [*Boufadel et al.*, 1999a; *Boufadel*, 2000]:

$$\phi S \frac{\partial c}{\partial t} = \beta[\nabla \cdot (\phi S \tau D_{\mathrm{m}} \nabla c) + \nabla \cdot (\mathbf{D} \nabla c)] - \mathbf{q} \cdot \nabla c, \tag{A7}$$

where $\nabla = \left(\frac{\partial}{\partial x}, \frac{\partial}{\partial z}\right)$ is the gradient operator with respect to the dimensional spatial variables, $\mathbf{q} = (q_x, q_z)$ [LT^{-1}] is the Darcy flux vector defined as:

$$\mathbf{q} = (q_x, q_z) = -\delta k_r K_0 \left(\frac{\partial \psi}{\partial x}, \frac{\partial \psi}{\partial z} + \beta\right), \tag{A8}$$

the term τ (dimensionless) is the domain tortuosity, D_{m} [L^{2}T^{-1}] is the diffusion coefficient (molecular diffusion). The term $\mathbf{D}$ in (A7) represents the dispersion tensor given by

$$\mathbf{D} = \frac{1}{\| \mathbf{q} \|} \begin{pmatrix} \alpha_L q_x^2 + \alpha_T q_z^2 & (\alpha_L - \alpha_T) q_x q_z \\ (\alpha_L - \alpha_T) q_x q_z & \alpha_T q_x^2 + \alpha_L q_z^2 \end{pmatrix}, \tag{A9}$$

where $\|\mathbf{q}\| = \sqrt{q_x^2 + q_z^2}$, α_L [L] and α_T [L] are the longitudinal and transverse dispersivities, respectively.

Appendix B

B1. Effect of Pits

[65] When the hydraulic conductivity in each pit was increased from 10^{-3} m/s (Model 1) to 5×10^{-3} m/s (Model 5) at W1 and W2, and from 10^{-2} m/s (Model 1) to 5×10^{-2} m/s (Model 5) at W3, W4 and W5, the match between the observed and simulated salinity of Model 5 became worse than that of Model 1 at wells W3 (Figure B1a), W4 (Figure B1b and Figure B1c) and W5 (Figure B1d). The salinities simulated by Model 5 are much higher than the observed ones, but those by Model 1 are reasonably close to

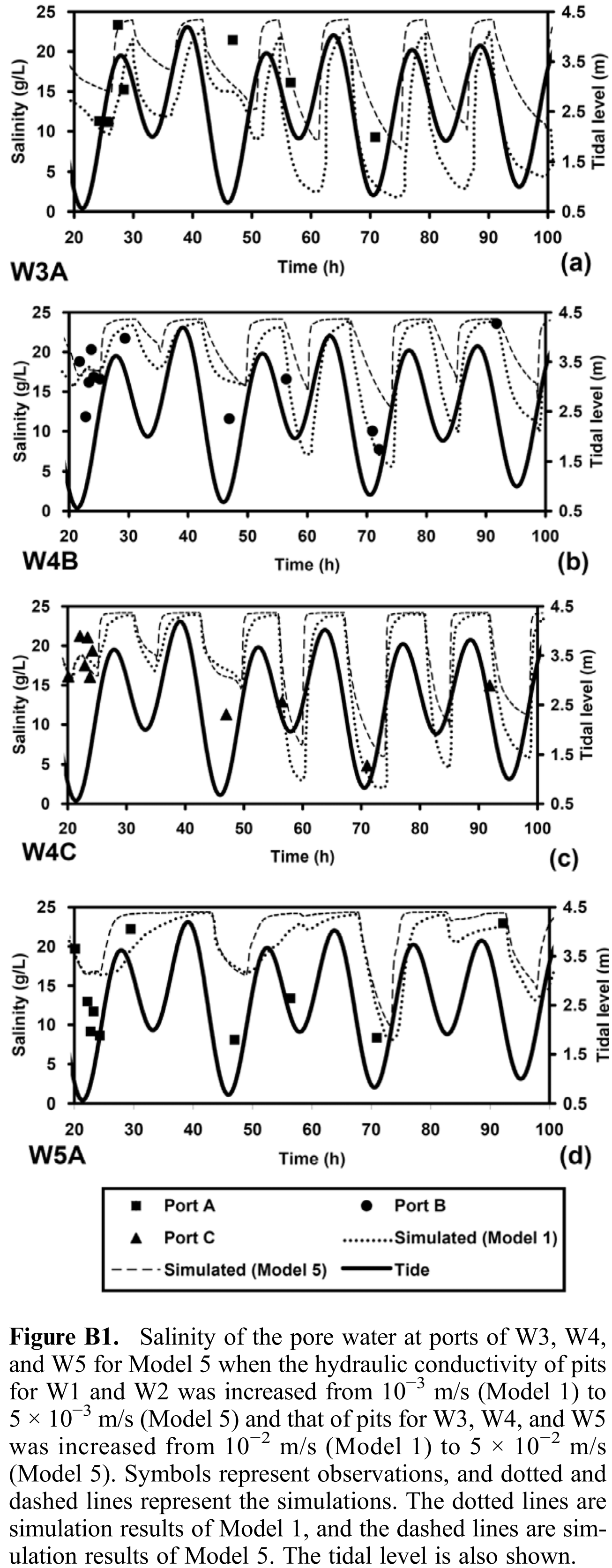

Figure B1. Salinity of the pore water at ports of W3, W4, and W5 for Model 5 when the hydraulic conductivity of pits for W1 and W2 was increased from 10^{-3} m/s (Model 1) to 5×10^{-3} m/s (Model 5) and that of pits for W3, W4, and W5 was increased from 10^{-2} m/s (Model 1) to 5×10^{-2} m/s (Model 5). Symbols represent observations, and dotted and dashed lines represent the simulations. The dotted lines are simulation results of Model 1, and the dashed lines are simulation results of Model 5. The tidal level is also shown.

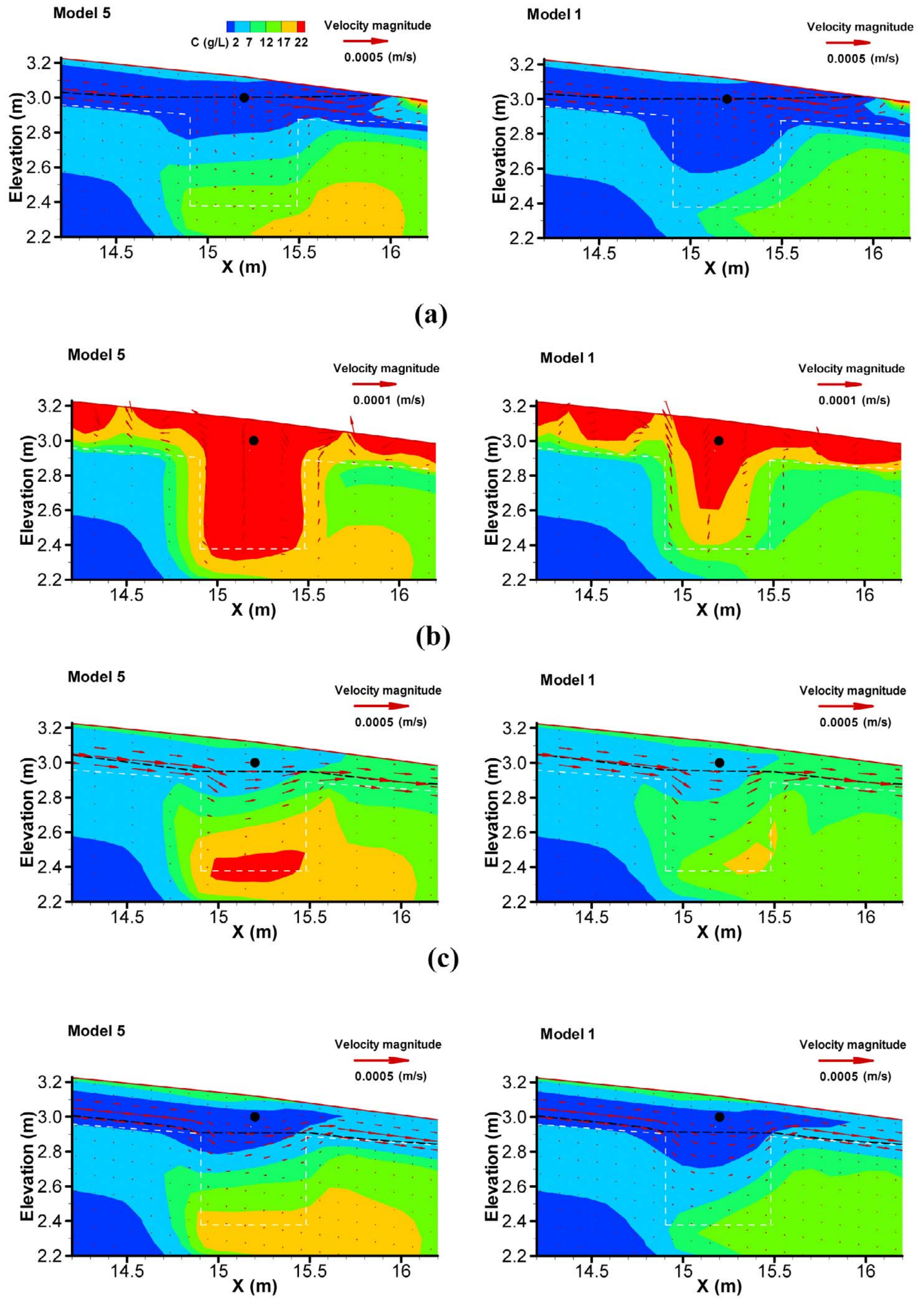

Figure B2. Simulated spatial salinity distributions and water table (black dashed lines) of Model 5 and Model 1 at different times of (a) rising midtide (t = 86 h), (b) high tide (t = 89 h), (c) falling midtide (t = 92 h), and (d) low tide (t = 95 h). The interface between the surface layer and the lower layer together with the pit at W3 is indicated by the white dashed line. The black circle represents the port C at W3.

the observed ones at Port A of W3, Ports B and C of W4, and Port A of W5, particularly at Ports B and C of W4. Take a typical time at t = 25 h of Port A at W3 as an example (Figure B1a), the error between the simulated salinity by Model 5 and the observation is around 4 g/L, whereas the error between the simulated salinity by Model 1 and observation is only 1 g/L. The relative error of Model 5 is 34%, much higher than that of Model 1 (10%). These results indicate that the hydraulic conductivities of pits in Model 5 are too high, resulting in more seawater (saltwater) entering the pits during rising tides than occurred in reality.

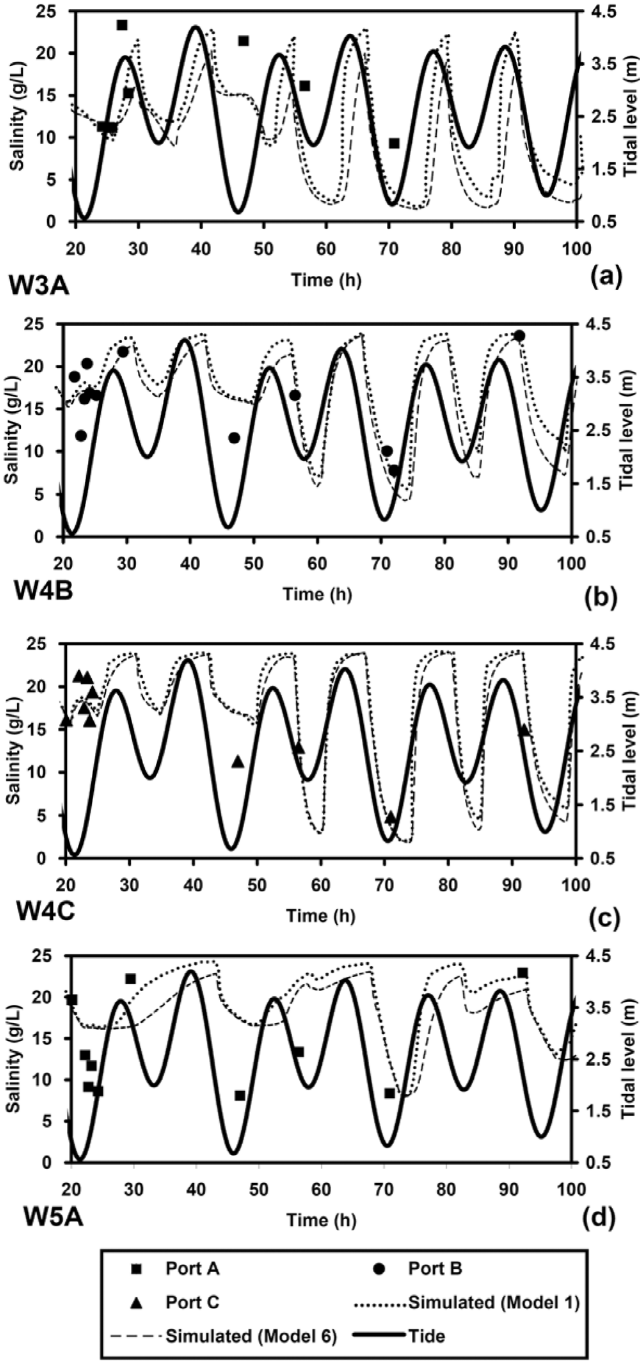

Figure B3. Salinity of the pore water at ports of W3, W4, and W5 for Model 6 when the hydraulic conductivity of pits for W1 and W2 was decreased from 10^{-3} m/s (Model 1) to 5×10^{-4} m/s (Model 6) and that of pits for W3, W4, and W5 was decreased from 10^{-2} m/s (Model 1) to 5×10^{-3} m/s (Model 6). Symbols represent observations, and dotted and dashed lines represent the simulations. The dotted lines are simulation results of Model 1, and the dashed lines are simulation results of Model 6. The tidal level is also shown.

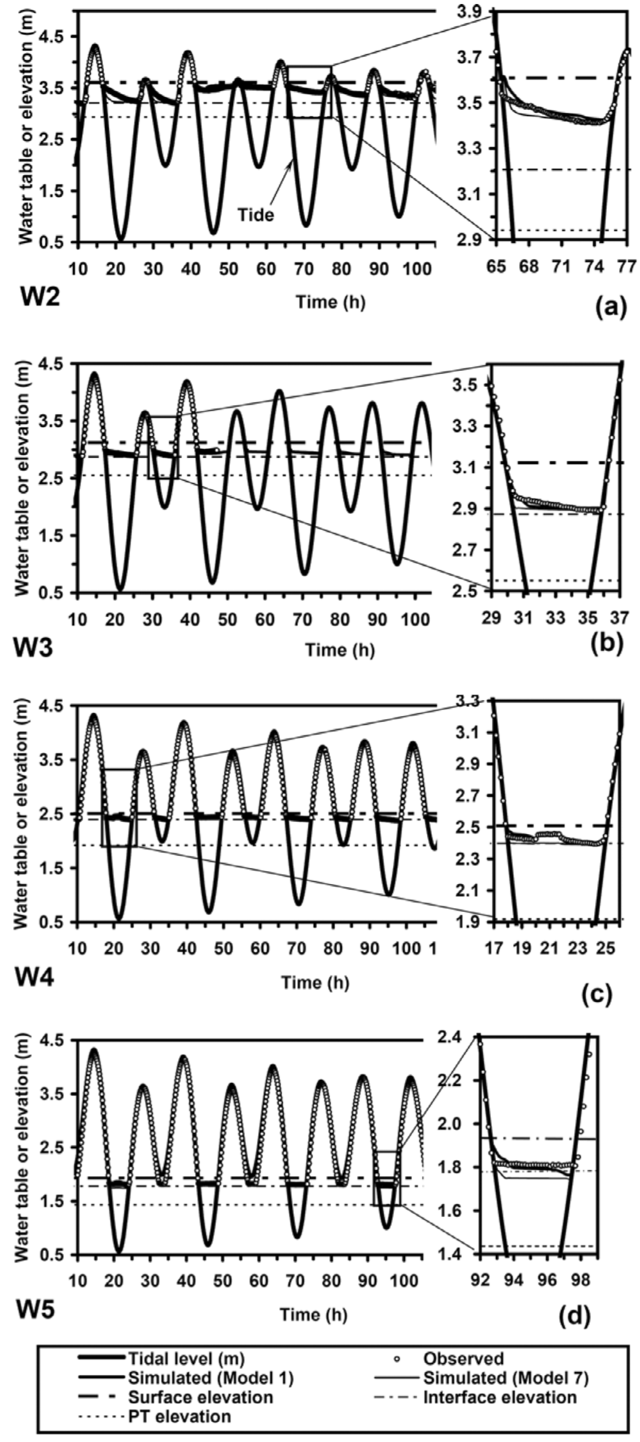

Figure B4. The water table at wells W2, W3, W4, and W5 when the hydraulic conductivity of the surface layer was increased from 10^{-3} m/s (Model 1) to 5×10^{-3} m/s (Model 7) for 0 m < x < 12 m and from 10^{-2} m/s (Model 1) to 5×10^{-2} m/s (Model 7) for 12 m < x < 70 m. Symbols represent observations, and solid lines represent the simulations. The thick solid lines are simulation results of Model 1, and the thin solid lines are simulation results of Model 7. The tidal level and the elevations of the beach surface, of the interface between the surface and the lower layers, and of the PTs (pressure transducers) installed at these observation wells are also shown to indicate the submersion period.

[66] At ports located in the shallow part of the pits (such as Port C of W2, Port C of W3 and Port B of W5), the difference of the salinities simulated by both Models 1 and 5

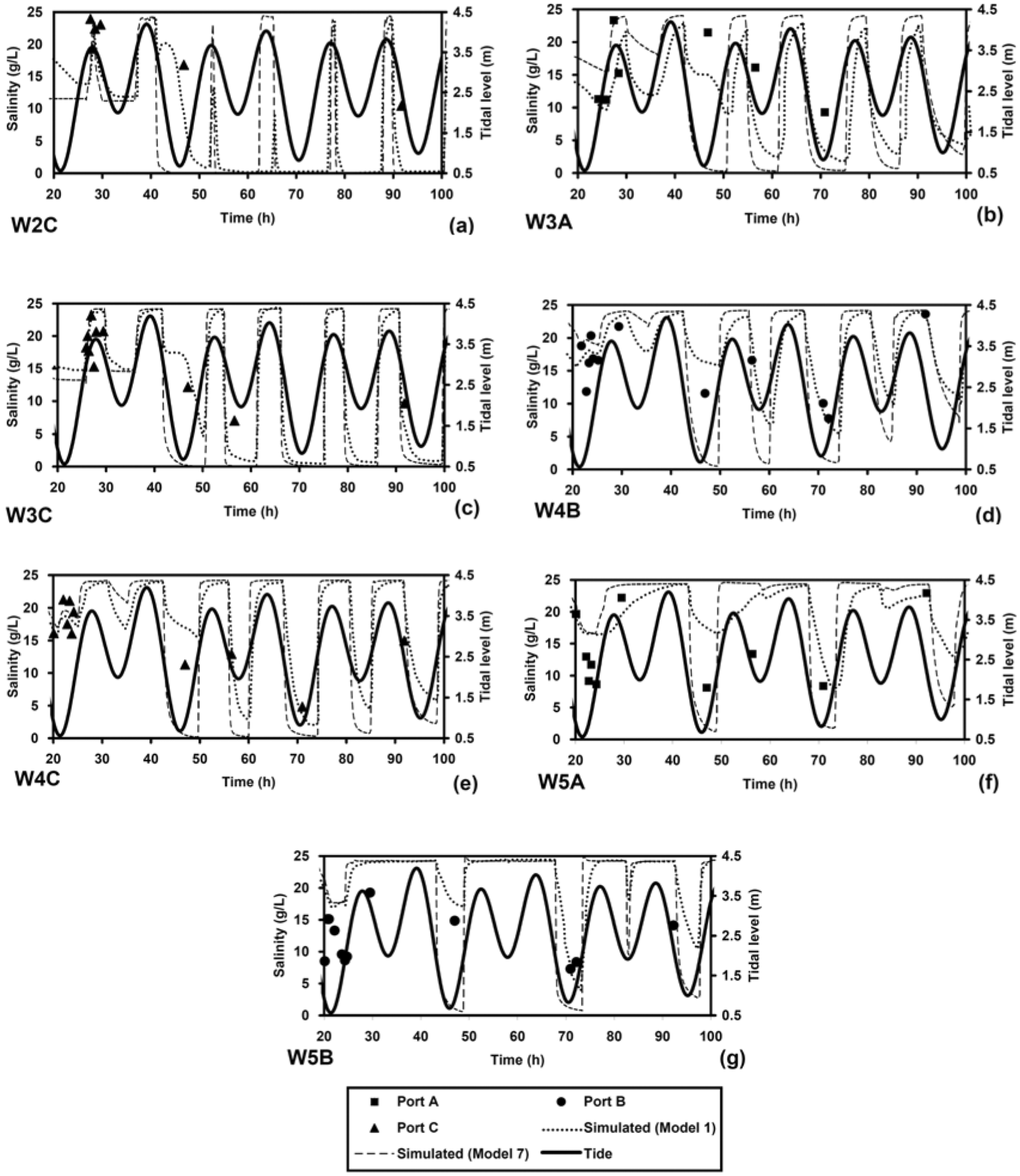

Figure B5. Salinity of pore water at ports of W2, W3, W4, and W5 when the hydraulic conductivity of the surface layer was increased from 10^{-3} m/s (Model 1) to 5×10^{-3} m/s (Model 7) for 0 m < x < 12 m and from 10^{-2} m/s (Model 1) to 5×10^{-2} m/s (Model 7) for 12 m < x < 70 m. Symbols represent observations, and dotted and dashed lines represent the simulations. The dotted lines are simulation results of Model 1, and the dashed lines are simulation results of Model 7. The tidal level is also shown to indicate the submersion period.

was very small (the results of time series are not shown here). It can be seen from Figure B2, where the salinity around port C of W3 was shown when it was submerged at t = 86 h (Figure B2a) and 89 h (Figure B2b), and emerged at t = 92 h (Figure B2c) and 95 h (Figure B2d). The salinity contours around port C (located at x = 15.20 m and z = 3.0 m) simulated by Models 1 and 5 are almost the same. During high tides, due to the shallow depth, it was easy for the front of seawater to arrive at these ports for the two K values used in Models 1 and 5. During low tides, larger quantity of freshwater from inland arrived at these ports, resulting in low salinity in them for the two K values used in Models 1 and 5.

[67] The water table was almost insensitive to the increasing of the hydraulic conductivity of pits. Due to the high permeability of the pits and the much low permeability of the lower layer both in Models 1 and 5, the water table in the pits was mainly determined by the elevation of the lowest intersection (most seaward) between the pit wall and the interface of the two layers. This was clearly demonstrated in Figure B2d, where the water table in the pit at low tide around t = 95 h was the same for Models 1 and 5.

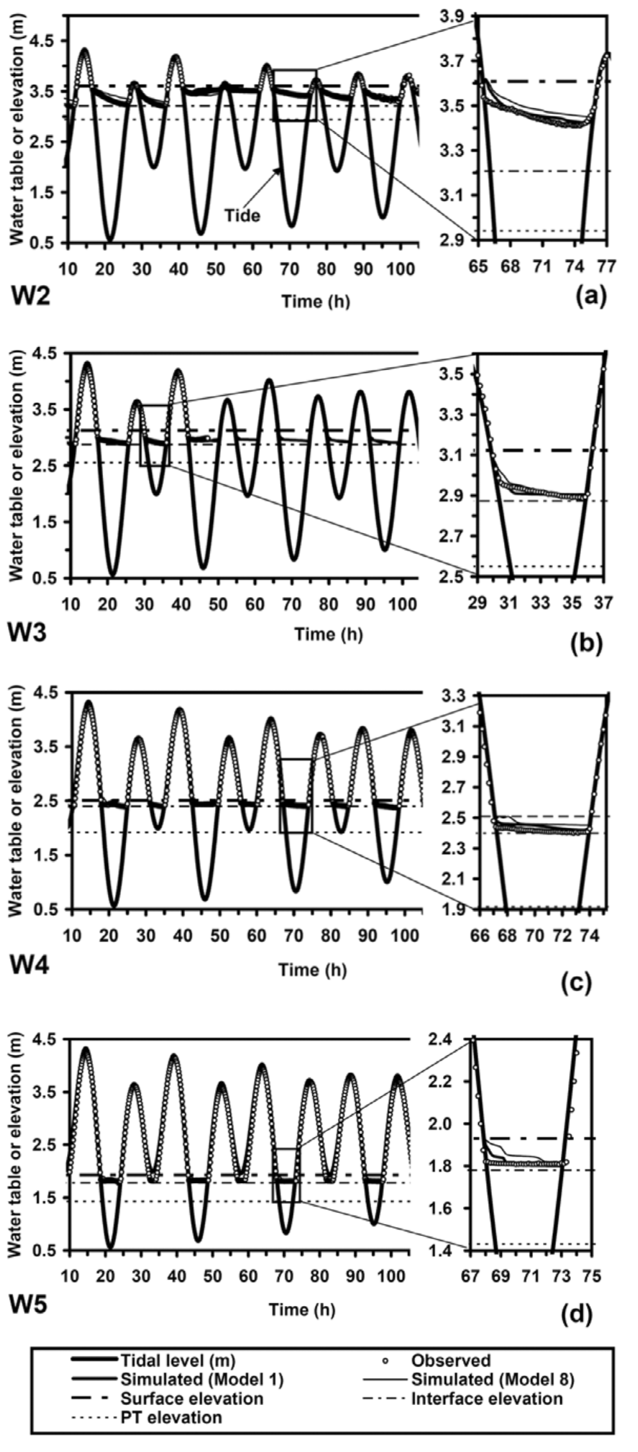

Figure B6. The water table at wells W2, W3, W4, and W5 for Model 8 when the hydraulic conductivity of the surface layer was decreased from 10^{-3} m/s (Model 1) to 5×10^{-4} m/s (Model 8) for 0 m < x < 12 m and from 10^{-2} m/s (Model 1) to 5×10^{-3} m/s (Model 8) for 12 m < x < 70 m. Symbols represent observations, and solid lines represent the simulations. The thick solid lines are simulation results of Model 1, and the thin solid lines are simulation results of Model 8. The tidal level and the elevations of the beach surface, of the interface between the surface and the lower layers, and of the PTs (pressure transducers) installed at these observation wells are also shown to indicate the submersion period.

[68] When the hydraulic conductivity in each pit was decreased from 10^{-3} m/s (Model 1) to 5×10^{-4} m/s (Model 6) at pits W1 and W2, and from 10^{-2} m/s (Model 1) to 5×10^{-3} m/s (Model 6) at pits W3, W4 and W5, the comparison between simulated and observed salinities deteriorated from that obtained by Model 1 at wells W3 (Figure B3a), W4 (Figure B3b and Figure B3c), and W5 (Figure B3d). The simulated salinities of Model 6 were lower than the observed ones at Port A of W3, Ports B and C of W4 and Port A of W5 near high tides. This indicates that the hydraulic conductivities of the pits of Model 6 are too low, resulting in less seawater (salt) entering into the pits.

[69] Similar to the situations discussed above, at locations in the shallow part of the pits (such as Port C of W2, Port C of W3 and Port B of W5), the difference of the salinities simulated by both Models 1 and 6 was very small (the results of time series are not shown here). The reason for this is similar to that discussed above (Figure B2). In addition, due to the same mechanism described above (Figure B2d), the decreasing of the hydraulic conductivity of pit had no effects on the water table at wells W2–W5.

B2. Surface Layer

[70] When the hydraulic conductivity in the surface layer was increased from 10^{-3} m/s (Model 1) to 5×10^{-3} m/s (Model 7) for 0.0 m < x < 12 m, and from 10^{-2} m/s (Model 1) to 5×10^{-2} m/s (Model 7) for 12 m < x < 70 m, the match to the observed water table by the simulation of Model 7 became worse than that of Model 1 (Figure B4). The water table simulated by Model 7 dropped faster than that by Model 1 during falling tides, indicating that the hydraulic conductivity of the surface layer used in Model 7 is too high.

[71] The match to the observed salinities by the simulation of Model 7 is considerably worse than that of Model 1 (Figure B5). The simulated salinities by Model 7 were higher than the observed ones near high tides, and lower than the observed ones near low tides at each port. These results demonstrated that much more seawater than in reality entered the surface layer and arrived at the monitoring locations during high tides, and much more freshwater than in reality, during low tides, indicating that the hydraulic conductivity of the surface layer in Model 7 is too high.

[72] When the hydraulic conductivity in the surface layer was decreased from 10^{-3} m/s (Model 1) to 5×10^{-4} m/s (Model 8) for 0 m < x < 12 m, and from 10^{-2} m/s (Model 1) to 5×10^{-3} m/s (Model 8) for 12 m < x < 70 m, the water table simulated by Model 8 were obviously worse than those by Model 1. The water table of Model 8 dropped more slowly during falling tides than the observed water table or the simulated by Model 1 (Figure B6). In particular, seepage face occurred at W4 (the water table located at the surface), which was not the case in reality. These results indicate that the hydraulic conductivities of the surface layer in Model 8 are too low to drain the pore water in the surface layer in time as in reality.

[73] The match to the observed salinities by Model 8 is considerably worse than that by Model 1 (Figure B7). The simulated salinities by Model 8 were higher than the observed ones near low tides, indicating that the hydraulic conductivity of the surface layer in Model 8 is too low to provide enough freshwater for diluting the pore water.

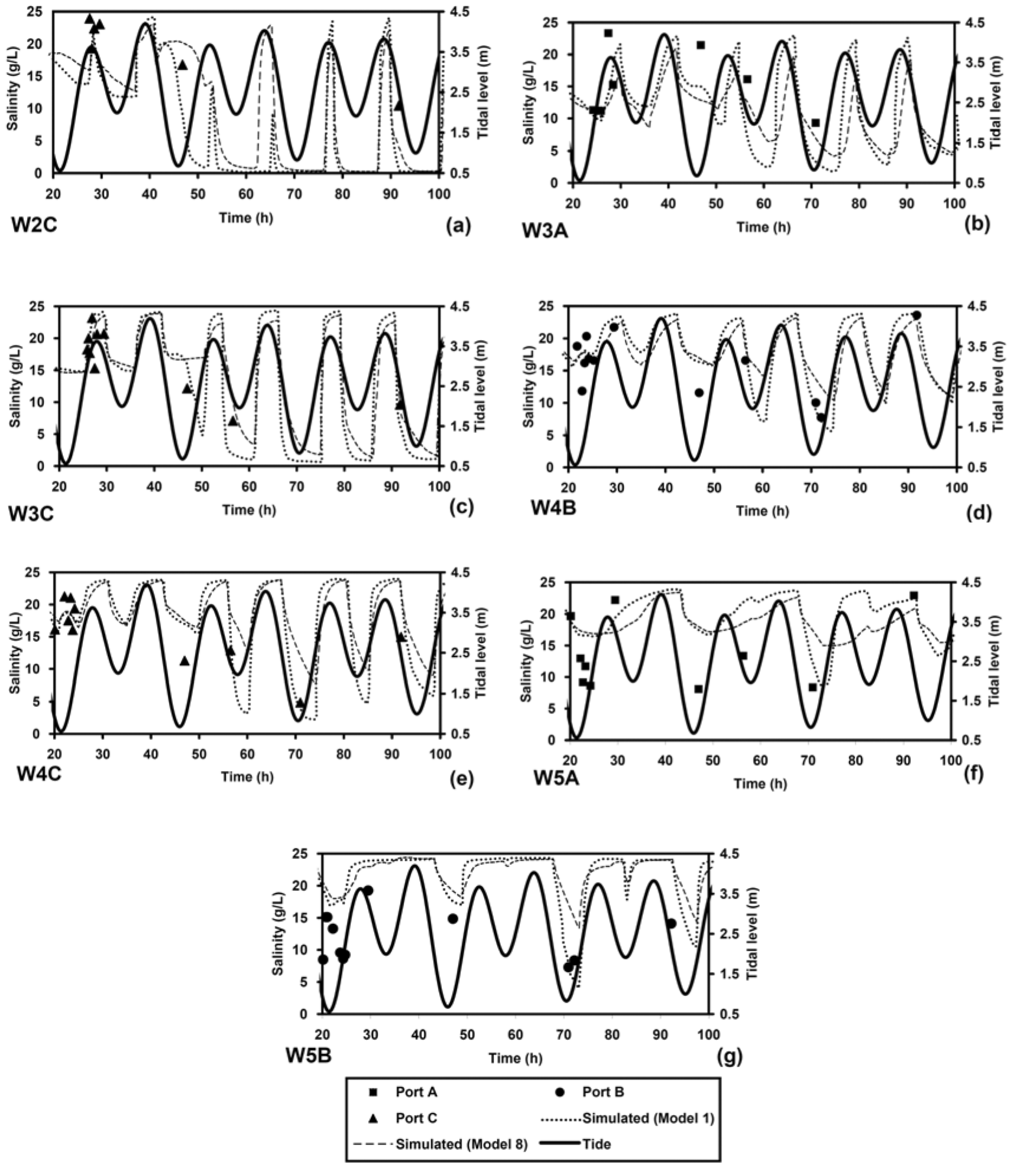

Figure B7. Salinity of the pore water at ports of W2, W3, W4, and W5 when the hydraulic conductivity of the surface layer was decreased from 10^{-3} m/s (Model 1) to 5×10^{-4} m/s (Model 8) for 0 m < x < 12 m and from 10^{-2} m/s (Model 1) to 5×10^{-3} m/s (Model 8) for 12 m < x < 70 m. Symbols represent observations, and dotted and dashed lines represent the simulations. The dotted lines are simulation results of Model 1, and the dashed lines are simulation results of Model 8. The tidal level is also shown.

[74] **Acknowledgments.** This work was supported in part by the Exxon Valdez Oil Spill Trustee Council (070836). The first author was supported by the "111 Project" of China (B08030). The first author is grateful to the State Scholarship Fund of China for its financial support. The work does not necessarily reflect the views of the funding entities, and no official endorsement should be inferred.

References

Ataie-Ashtiani, B., R. E. Volker, and D. A. Lockington (1999), Tidal effects on sea water intrusion in unconfined aquifers, *J. Hydrol.*, *216*(1–2), 17–31, doi:10.1016/S0022-1694(98)00275-3.

Ataie-Ashtiani, B., R. E. Volker, and D. A. Lockington (2001), Tidal effects on groundwater dynamics in unconfined aquifers, *Hydrol. Processes*, *15*(4), 655–669, doi:10.1002/hyp.183.

Atlas, R., and J. R. Bragg (2009), Evaluation of PAH depletion of subsurface Exxon Valdez oil residues remaining in Prince William sound in 2007–2008 and their likely bioremediation potential, in *Proceedings of the 32nd AMOP Technical Seminar on Environmental Contamination and Response*, vol. 2, pp. 723–747, Emergencies Sci. Div., Environ. Canada, Ottawa.

Bear, J. (1988), *Dynamics of Flow in Porous Media*, 764 pp., Dover, New York.

Bodin, P. (1988), Results of ecological monitoring of three beaches polluted by the Amoco Cadiz oil spill development of meiofauna from 1978 to 1984, *Mar. Ecol. Prog. Ser.*, *42*, 105–123, doi:10.3354/meps042105.

Boehm, P. D., D. S. Page, J. M. Neff, and C. B. Johnson (2007), Potential for sea otter exposure to remnants of buried oil from the Exxon Valdez oil spill, *Environ. Sci. Technol.*, *41*(19), 6860–6867, doi:10.1021/es070829e.

Boufadel, M. C. (2000), A mechanistic study of nonlinear solute transport in a groundwater-surface water system under steady state and transient hydraulic conditions, *Water Resour. Res.*, *36*(9), 2549–2565, doi:10.1029/2000WR900159.

Boufadel, M. C., M. T. Suidan, C. H. Rauch, A. D. Venosa, and P. Biswas (1998), 2D variably saturated flow: Physical scaling and Bayesian estimation, *J. Hydrol. Eng.*, *3*, 223–231, doi:10.1061/(ASCE)1084-0699(1998)3:4(223).

Boufadel, M. C., M. T. Suidan, and A. D. Venosa (1999a), A numerical model for density-and-viscosity-dependent flows in two-dimensional variably saturated porous media, *J. Contam. Hydrol.*, *37*(1–2), 1–20, doi:10.1016/S0169-7722(98)00164-8.

Boufadel, M. C., M. T. Suidan, and A. D. Venosa (1999b), Numerical modeling of water flow below dry salt lakes: Effect of capillarity and viscosity, *J. Hydrol.*, *221*(1–2), 55–74, doi:10.1016/S0022-1694(99)00077-3.

Boufadel, M. C., M. T. Suidan, A. D. Venosa, and M. T. Bowers (1999c), Steady seepage in trenches and dams: Effect of capillary flow, *J. Hydrol. Eng.*, *125*, 286–294, doi:10.1061/(ASCE)0733-9429(1999)125:3(286).

Boufadel, M. C., M. T. Suidan, and A. D. Venosa (2006), Tracer studies in laboratory beach simulating tidal influences, *J. Environ. Eng.*, *132*(6), 616–623, doi:10.1061/(ASCE)0733-9372(2006)132:6(616).

Boufadel, M. C., H. Li, M. T. Suidan, and A. D. Venosa (2007), Tracer studies in a laboratory beach subjected to waves, *J. Environ. Eng.*, *133*(7), 722–732, doi:10.1061/(ASCE)0733-9372(2007)133:7(722).

Bragg, J. R., R. C. Prince, E. J. Harner, and R. M. Atlas (1994), Effectiveness of bioremediation for the *Exxon Valdez* oil spill, *Nature*, *368*, 413–418, doi:10.1038/368413a0.

Brovelli, A., X. Mao, and D. A. Barry (2007), Numerical modeling of tidal influence on density-dependent contaminant transport, *Water Resour. Res.*, *43*, W10426, doi:10.1029/2006WR005173.

Buscombe, D., and G. Masselink (2006), Concepts in gravel beach dynamics, *Earth Sci. Rev.*, *79*(1–2), 33–52, doi:10.1016/j.earscirev.2006.06.003.

Carrier, W. D. (2003), Goodbye, Hazen; hello, Kozeny-Carman, *J. Geotech. Geoenviron. Eng.*, *129*(11), 1054–1056, doi:10.1061/(ASCE)1090-0241(2003)129:11(1054).

Cartwright, N., O. Z. Jessen, and P. Nielsen (2006), Application of a coupled ground-surface water flow model to simulate periodic groundwater flow influenced by a sloping boundary, capillarity and vertical flows, *Environ. Modell. Softw.*, *21*(6), 770–778, doi:10.1016/j.envsoft.2005.02.005.

Church, T. M. (1996), An underground route for the water cycle, *Nature*, *380*, 579–580, doi:10.1038/380579a0.

Coyle, K. O., and A. I. Pinchuk (2005), Seasonal cross-shelf distribution of major zooplankton taxa on the northern Gulf of Alaska shelf relative to water mass properties, species depth preferences and vertical migration behavior, *Deep Sea Res., Part II*, *52*, 217–245, doi:10.1016/j.dsr2. 2004.09.025.

Croucher, A. E., and M. J. O'Sullivan (1995), The Henry problem for saltwater intrusion, *Water Resour. Res.*, *31*, 1809–1814, doi:10.1029/95WR00431.

Destouni, G., and C. Prieto (2003), On the possibility for generic modelling of submarine groundwater discharge, *Biogeochemistry*, *66*, 171–186, doi:10.1023/B:BIOG.0000006101.12076.10.

Duxbury, A. B., and A. C. Duxbury (2001), *Fundamentals of Oceanography*, 4th ed., McGraw-Hill, New York.

Elder, J. W. (1967), Transient convection in a porous medium, *J. Fluid Mech.*, *27*, 609–623, doi:10.1017/S0022112067000576.

Eljamal, O., K. Jinno, and T. Hosokawa (2008), Modeling of solute transport with bioremediation processes using sawdust as a matrix, *Water Air Soil Pollut.*, *195*(1–4), 115–127, doi:10.1007/s11270-008-9731-y.

Frind, E. O. (1982), Simulation of long-term transient density-dependent transport in groundwater, *Adv. Water Resour.*, *5*, 73–88, doi:10.1016/0309-1708(82)90049-5.

Galeati, G., G. Gambolati, and S. P. Neuman (1992), Coupled and partially coupled Eulerian-Lagrangian model of freshwater-seawater mixing, *Water Resour. Res.*, *28*(1), 149–165, doi:10.1029/91WR01927.

Gelhar, L. W., and C. L. Axness (1983), Three-dimensional stochastic analysis of macrodispersion in aquifers, *Water Resour. Res.*, *19*, 161–180, doi:10.1029/WR019i001p00161.

Hayes, M. O., J. Michel, and D. V. Betenbaugh (2009), The intermittently exposed, coarse-grained gravel beaches of Prince William Sound, Alaska: Comparison with open-ocean gravel beaches, *J. Coastal Res.*, *26*, 4–30.

Horn, D. P. (2002), Beach groundwater dynamics, *Geomorphology*, *48*(1–3), 121–146, doi:10.1016/S0169-555X(02)00178-2.

Horn, D. P., and S. M. Walton (2007), Spatial and temporal variations of sediment size on a mixed sand and gravel beach, *Sediment. Geol.*, *202*(3), 509–528, doi:10.1016/j.sedgeo.2007.03.023.

Jeng, D. S., X. Mao, P. Enot, D. A. Barry, and L. Li (2005), Spring-neap tide-induced beach water table fluctuations in a sloping coastal aquifer, *Water Resour. Res.*, *41*, W07026, doi:10.1029/2005WR003945.

Li, H., and M. C. Boufadel (2010), Long-term persistence of oil from the *Exxon Valdez* spill in two-layer beaches, *Nat. Geosci.*, *3*, 96–99, doi:10.1038/ngeo749.

Li, H. L., L. Li, and D. Lockington (2005), Aeration for plant root respiration in a tidal marsh, *Water Resour. Res.*, *41*, W06023, doi:10.1029/2004WR003759.

Li, H. L., Q. H. Zhao, M. C. Boufadel, and A. D. Venosa (2007), A universal nutrient application strategy for the bioremediation of oil polluted beaches, *Mar. Pollut. Bull.*, *54*, 1146–1161, doi:10.1016/j.marpolbul.2007.04.015.

Li, H., M. C. Boufadel, and J. W. Weaver (2008), Tide-induced seawater-groundwater circulation in shallow beach aquifers, *J. Hydrol.*, *352*(1–2), 211–224, doi:10.1016/j.jhydrol.2008.01.013.

Li, L., D. A. Barry, F. Stagnitti, and J. Y. Parlange (1999), Submarine groundwater discharge and associated chemical input to a coastal sea, *Water Resour. Res.*, *35*(11), 3253–3259, doi:10.1029/1999WR900189.

Li, L., D. A. Barry, F. Stagnitti, J. Y. Parlange, and D. S. Jeng (2000), Beach water table fluctuations due to spring-neap tides: Moving boundary effects, *Adv. Water Resour.*, *23*(8), 817–824, doi:10.1016/S0309-1708(00)00017-8.

Mao, X., P. Enot, D. A. Barry, L. Li, A. Binley, and D. S. Jeng (2006), Tidal influence on behaviour of a coastal aquifer adjacent to a low-relief estuary, *J. Hydrol.*, *327*(1–2), 110–127, doi:10.1016/j.jhydrol.2005.11.030.

McLachlan, A., and I. Turner (1994), The interstitial environment of sandy beaches, *Mar. Ecol.*, *15*(3–4), 177–211.

Melchior, P. (1964), Earth tides, *Res. Geophys.*, vol. 2, edited by H. Odishaw, pp. 163–193, MIT Press, Cambridge, Mass.

Merritt, M. L. (2004), Estimating hydraulic properties of the Floridian aquifer system by analysis of Earth-tide, ocean-tide, and barometric effects, Collier and Hendry counties, Florida, *U.S. Geol. Surv. Water Resour. Invest. Rep.*, *03-4267*, 4203–4267.

Michael, H. A., A. E. Mulligan, and C. F. Harvey (2005), Seasonal oscillations in water exchange between aquifers and the coastal ocean, *Nature*, *436*(7054), 1145–1148, doi:10.1038/nature03935.

Miller, D. C., and W. J. Ullman (2004), Ecological consequences of ground water discharge to Delaware Bay, United States, *Ground Water*, *42*(7), 959–970, doi:10.1111/j.1745-6584.2004.tb02635.x.

Moore, W. S. (1999), The subterranean estuary: A reaction zone of ground water and sea water, *Mar. Chem.*, *65*(1–2), 111–125, doi:10.1016/S0304-4203(99)00014-6.

Naba, B., M. C. Boufadel, and J. W. Weaver (2002), The role of capillary forces in steady-state and transient seepage flows, *Ground Water*, *40*(4), 407–415, doi:10.1111/j.1745-6584.2002.tb02519.x.

Neff, J. M., E. H. Owens, S. W. Stoker, and D. M. McCormick (1995), Shoreline oiling conditions in Prince William Sound following the *Exxon Valdez* oil spill, in *Exxon Valdez Oil Spill: Fate and Effects in Alaskan Waters, STP 1219*, edited by P. G. Wells, J. N. Butler, and J. S. Hughes, pp. 312–346, Am. Soc. for Test. and Mater., Philadelphia, Pa., doi:10.1520/STP19869S.

Neuman, S. P. (1990), Universal scaling of hydraulic conductivities and dispersivities in geologic media, *Water Resour. Res.*, *26*(8), 1749–1758, doi:10.1029/WR026i008p01749.

Nielsen, P. (1990), Tidal dynamics of the water table in beaches, *Water Resour. Res.*, *26*(9), 2127–2134.

Owens, E. H., E. Taylor, and B. Humphrey (2008), The persistence and character of stranded oil on coarse-sediment beaches, *Mar. Pollut. Bull.*, *56*(1), 14–26, doi:10.1016/j.marpolbul.2007.08.020.

Rajaram, H., and L. W. Gelhar (1993), Plume scale-dependent dispersion in heterogeneous aquifers: 2. Eulerian analysis and three-dimensional aquifers, *Water Resour. Res.*, *29*(9), 3261–3276, doi:10.1029/93WR01068.

Robinson, C., B. Gibbes, and L. Li (2006), Driving mechanisms for groundwater flow and salt transport in a subterranean estuary, *Geophys. Res. Lett.*, *33*, L03402, doi:10.1029/2005GL025247.

Robinson, C., B. Gibbes, H. Carey, and L. Li (2007), Salt-freshwater dynamics in a subterranean estuary over a spring-neap tidal cycle, *J. Geophys. Res.*, *112*, C09007, doi:10.1029/2006JC003888.

Robinson, M. A., and D. L. Gallagher (1999), A model of ground water discharge from an unconfined coastal aquifer, *Ground Water*, *37*(1), 80–87, doi:10.1111/j.1745-6584.1999.tb00960.x.

Robinson, M. A., D. Gallagher, and W. Reay (1998), Field observations of tidal and seasonal variations in ground water discharge to tidal estuarine surface water, *Ground Water Monit. Rem.*, *18*(1), 83–92, doi:10.1111/j.1745-6592.1998.tb00605.x.

Short, J. W., M. R. Lindeberg, P. M. Harris, J. M. Maselko, J. J. Pella, and S. D. Rice (2004), Estimate of oil persisting on the beaches of Prince William Sound 12 years after the *Exxon Valdez* oil spill, *Environ. Sci. Technol.*, *38*(1), 19–25, doi:10.1021/es0348694.

Short, J. W., J. M. Maselko, M. R. Lindeberg, P. M. Harris, and S. D. Rice (2006), Vertical distribution and probability of encountering intertidal Exxon Valdez oil on shorelines of three embayments within Prince William Sound, Alaska, *Environ. Sci. Technol.*, *40*(12), 3723–3729, doi:10.1021/es0601134.

Taylor, E., and D. Reimer (2008), Oil persistence on beaches in Prince William Sound: A review of SCAT surveys conducted from 1989 to 2002, *Mar. Pollut. Bull.*, *56*(3), 458–474, doi:10.1016/j.marpolbul.2007.11.008.

Teo, H. T., D. S. Jeng, B. R. Seymour, D. A. Barry, and L. Li (2003), A new analytical solution for water table fluctuations in coastal aquifers with sloping beaches, *Adv. Water Resour.*, *26*(12), 1239–1247, doi:10.1016/j.advwatres.2003.08.004.

Turner, I. (1993), Water table outcropping on macro-tidal beaches: A simulation model, *Mar. Geol.*, *115*(3–4), 227–238, doi:10.1016/0025-3227(93)90052-W.

Turner, I. L., B. P. Coates, and R. I. Acworth (1997), Tides, waves and the super-elevation of groundwater at the coast, *J. Coastal Res.*, *13*(1), 46–60.

Ullman, W. J., B. Chang, D. C. Miller, and J. A. Madsen (2003), Groundwater mixing, nutrient diagenesis, and discharges across a sandy beachface, Cape Henlopen, Delaware (USA), *Estuarine Coastal Shelf Sci.*, *57*(3), 539–552, doi:10.1016/S0272-7714(02)00398-0.

van Genuchten, M. T. (1980), A closed-form equation for predicting the hydraulic conductivity of unsaturated soils, *Soil Sci. Soc. Am. J.*, *44*, 892–898, doi:10.2136/sssaj1980.03615995004400050002x.

Venosa, A. D., and X. Zhu (2003), Biodegradation of crude oil contaminating marine shorelines and freshwater wetlands, *Spill Sci. Technol. Bull.*, *8*, 163–178, doi:10.1016/S1353-2561(03)00019-7.

Venosa, A. D., M. T. Suidan, B. A. Wrenn, K. L. Strohmeier, J. R. Haines, B. L. Eberhart, D. King, and E. Holder (1996), Bioremediation of an experimental oil spill on the shoreline of Delaware Bay, *Environ. Sci. Technol.*, *30*(5), 1764–1775, doi:10.1021/es950754r.

Werner, A. D., and D. A. Lockington (2006), Tidal impacts on riparian salinities near estuaries, *J. Hydrol.*, *328*(3–4), 511–522, doi:10.1016/j.jhydrol.2005.12.011.

Wrenn, B. A., M. C. Boufadel, M. T. Suidan, and A. D. Venosa (1997), Nutrient transport during bioremediation of crude oil contaminated beaches, in *4th International Symposium on In-Situ and On-Site Bioremediation*, pp. 267–272, Battelle, Columbus, Ohio.

Xia, Y., H. Li, M. C. Boufadel, and Y. Sharifi (2010), Hydrodynamic factors affecting the persistence of the *Exxon Valdez* oil in a shallow bedrock beach, *Water Resour. Res.*, *46*, W10528, doi:10.1029/2010WR009179.

Younger, P. L. (1996), Submarine groundwater discharge, *Nature*, *382*, 121–122, doi:10.1038/382121a0.

M. C. Boufadel and Y. Sharifi, Department of Civil and Environmental Engineering, Temple University, 1947 N. 12th St., Philadelphia, PA 19122, USA. (boufadel@temple.edu)

Q. Guo and H. Li, School of Environmental Studies and (MOE) Biogeology and Environmental Geology Laboratory, China University of Geosciences, Wuhan 430074, China.